The Response of Stainless Steel to the Pellet Debris in a Laser Fusion Reactor

T. McCarville, A.M. Hassanein, and G.L. Kulcinski

December 1978

UWFDM-282

5th International SMiRT Conf., Berlin, Vol. N., P.N. 2.5/4, 1979.

FUSION TECHNOLOGY INSTITUTE

UNIVERSITY OF WISCONSIN

MADISON WISCONSIN

The Response of Stainless Steel to the Pellet Debris in a Laser Fusion Reactor

T. McCarville, A.M. Hassanein, and G.L. Kulcinski

Fusion Technology Institute
University of Wisconsin
1500 Engineering Drive
Madison, WI 53706

http://fti.neep.wisc.edu

December 1978

UWFDM-282

5th International SMiRT Conf., Berlin, Vol. N., P.N. 2.5/4, 1979.

THE RESPONSE OF STAINLESS STEEL TO THE PELLET DEBRIS IN A LASER FUSION REACTOR

T. J. McCarville
A. M. Hassanein
G. L. Kulcinski

November 1978

UWFDM-282

University of Wisconsin
Nuclear Engineering Department
Madison, Wisconsin 53706

The Response of Stainless Steel to the Pellet Debris in a Laser Fusion Reactor

1. Introduction

A method has been recently developed to calculate the time and spacial variations of the temperature and displacement transients associated with a radiation spectra on laser reactor first wall materials.[1,2,3] It was found that laser fusion pellet debris could promote very large temperature excursions in copper, molybdenum and carbon and that displacement rates could approach several hundred dpa/s in the near surface region. The object of the present study is to extend the previous investigations to a possible first wall construction material, stainless steel, which has a particularly low thermal conductivity. The main objectives of this analysis are:

1. To study the displacement, thermal response, and surface evaporation of stainless steel as a first wall material.
2. To study the effect of an inert buffer gas to protect stainless steel from X-rays and ions.

In this analysis the response models were applied to radiation spectra from the same structured pellet used in previous studies.[3]

2. Calculation Descriptions

The code used for this work, T*DAMEN,[4] calculates spacial and temporal energy deposition from a given pellet spectra, and uses the result as a heat source from which the spacial and temporal temperature response can be calculated. The displacement damage from each component of the spectra is also calculated. The consequences of significant energy deposition into the first wall, outlined in Figure 1, can lead

FIGURE 1

TRANSIENT DAMAGE ANALYSIS

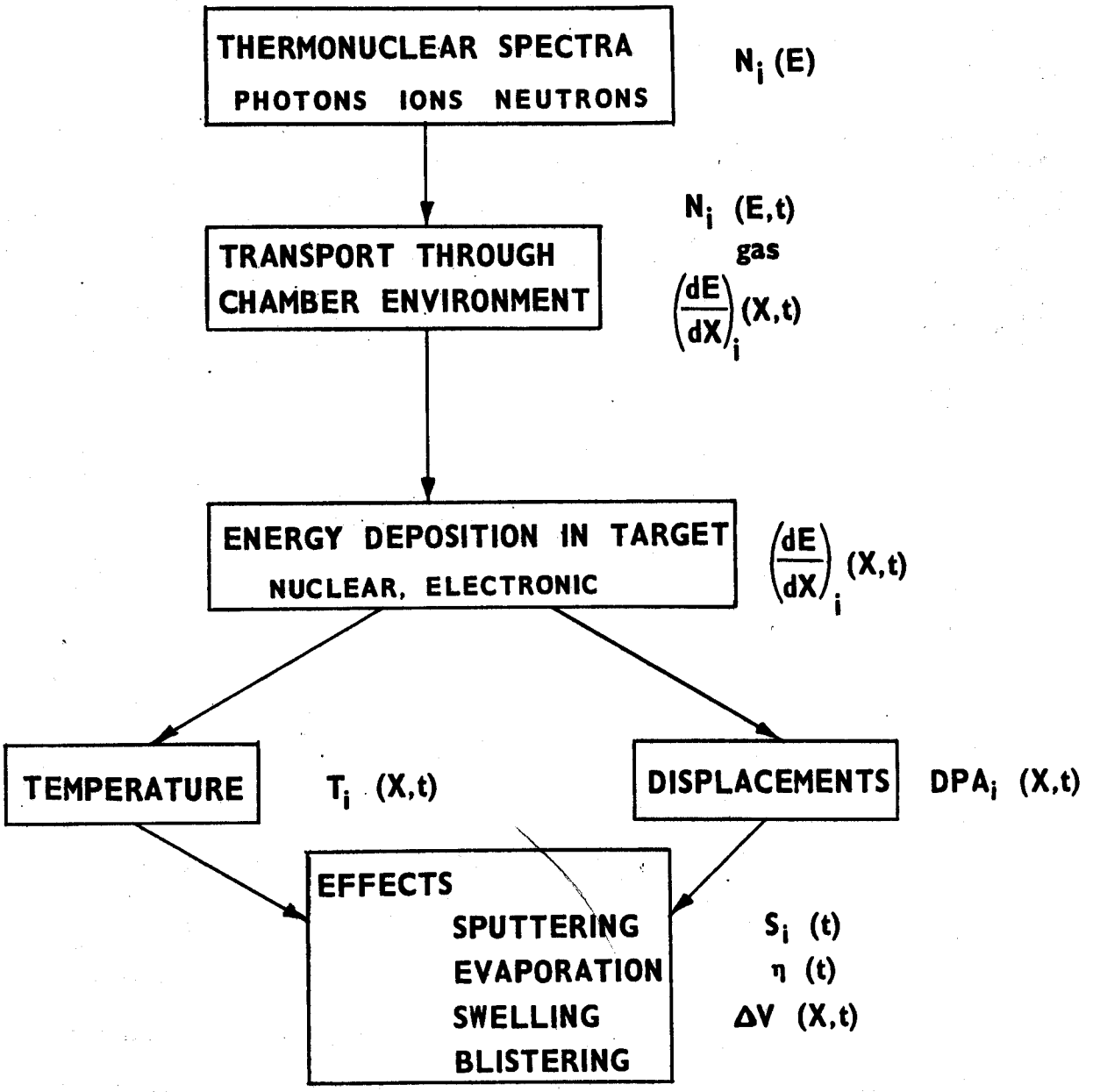

to enhanced sputtering, evaporation, and other effects detrimental to first wall life.

The notation outside of the block diagrams in Figure 1 indicates that given a photon and ion spectra originating at the point of micro-explosion, a gas layer can be used to modify the spectra during transport, resulting in reduced energy deposition and surface effects at the first wall. The model used to consider the effects of the buffering gas and calculate the modified spectrum into the first wall is based on a diffusion approximation to the transport theory solution.[3] Such approximations are useful for parameter studies where the effects of variations in gas types and pressures are investigated.

The results of two separate sets of calculations will be presented here. Both have assumed a spherical reactor geometry and a bare first wall having the thermal properties of stainless steel but the stopping power of nickel. At the present time these calculations do not incorporate changes in thermal constants with temperature and no latent heat melting is included. Therefore, temperatures above the melting point have little meaning and we report only the temperature increase above ambient, leaving it to the reader to determine where the validity of the results end.

The first set of data presented is the result of T*DAMEN calculations that consider a complete pellet spectrum consisting of light and heavy ions, reflected laser light, and X-rays. These calculations illustrate the effect that 0.5 torr of neon gas can have on the total damage and temperature excursions at the first wall. A description of the pellet spectrum, before modification by the gas, is given in Table I. The energy dependence of the spectra at the first wall and slowing down effects of gas are illustrated in Figure 2, with the exception of reflected laser

FIGURE 2

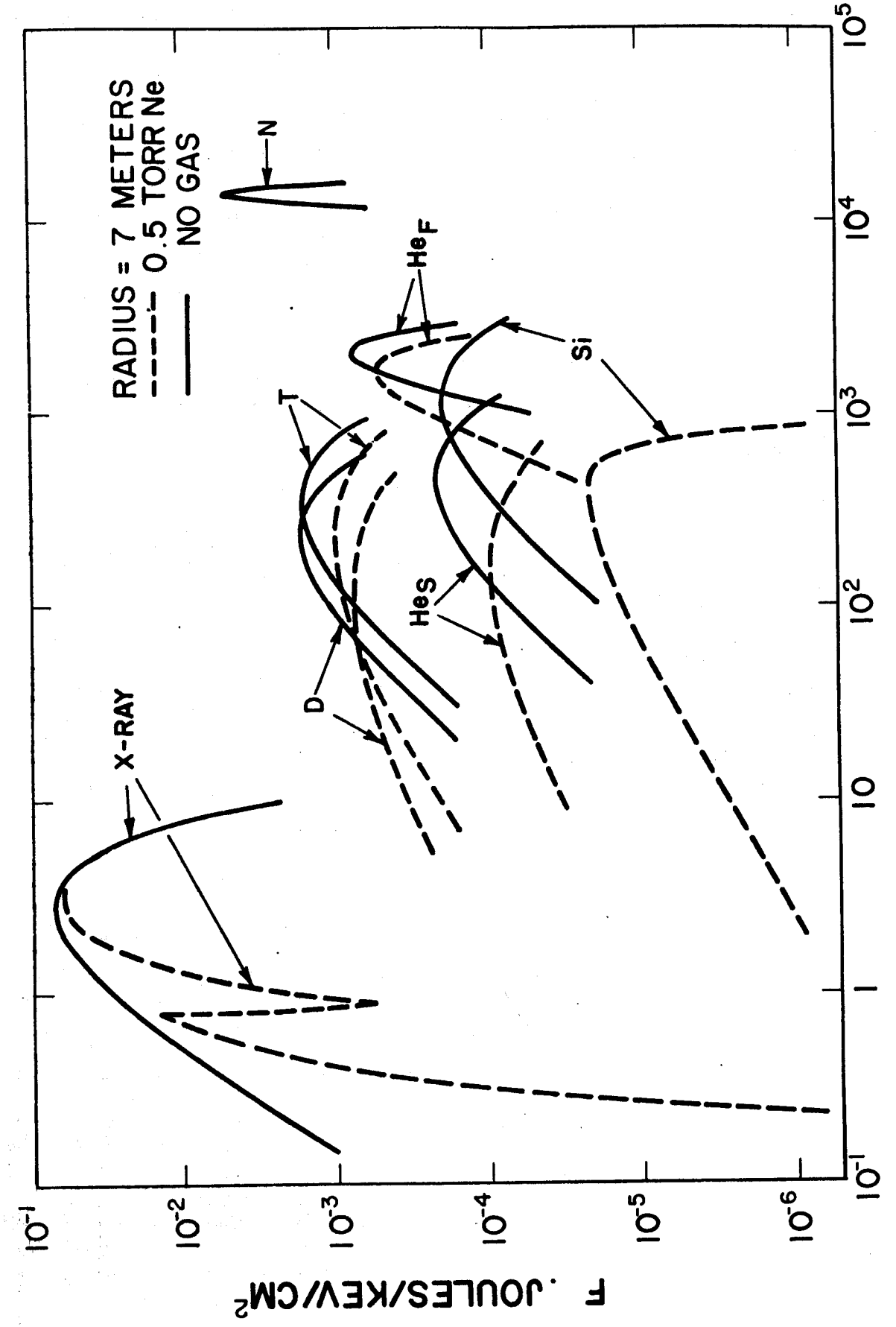
ENERGY SPECTRA - IONS AND X-RAYS
RADIUS = 7 METERS
0.5 TORR Ne
NO GAS
N
X-RAY
D
T
He_S
He_F
Si
F, JOULES/KEV/CM²
ENERGY, KEV
10⁻¹
10⁻²
10⁻³
10⁻⁴
10⁻⁵
10⁻⁶
1
10
10²
10³
10⁴
10⁵

Table I

REFERENCE SPECTRA (100 MJ)

	Energy (MJ)	Spectrum
Laser	.2	10.6 μ
X-ray	2	1.0 keV - BB
D	4.6	160 keV - M
T	6.9	240 keV - M
He (Slow)	1.2	320 keV - M
He (Fast)	5.4	2 ± .5 MeV - G
Silicon	2.7	800 keV - M
Neutrons	77.	14 ± 1 MeV - G

BB = Blackbody M = Maxwellian G = Gaussian

light, which is monenergetic and assumed to be unaffected by the gas. Although the neutrons possess most of the energy released by the micro-explosion, little of it is deposited at the first wall and for this reason temperature excursions from neutrons can be neglected for this study.

The time of arrival, and the effect that 0.5 torr of Ne gas has on that time, is represented in Figure 3. X-rays arrive at the first wall picoseconds after the burn (not shown in Figure 3), whereas ions arrive at times orders of magnitude larger. Hence the time of arrival for the pellet debris will be measured from the time of arrival of the first X-rays.

The second set of results presented is a parameter study showing the relative effectiveness of Xe, Ne, and He as a buffer gas at different

ION PARTICLE FLUX FIGURE 3

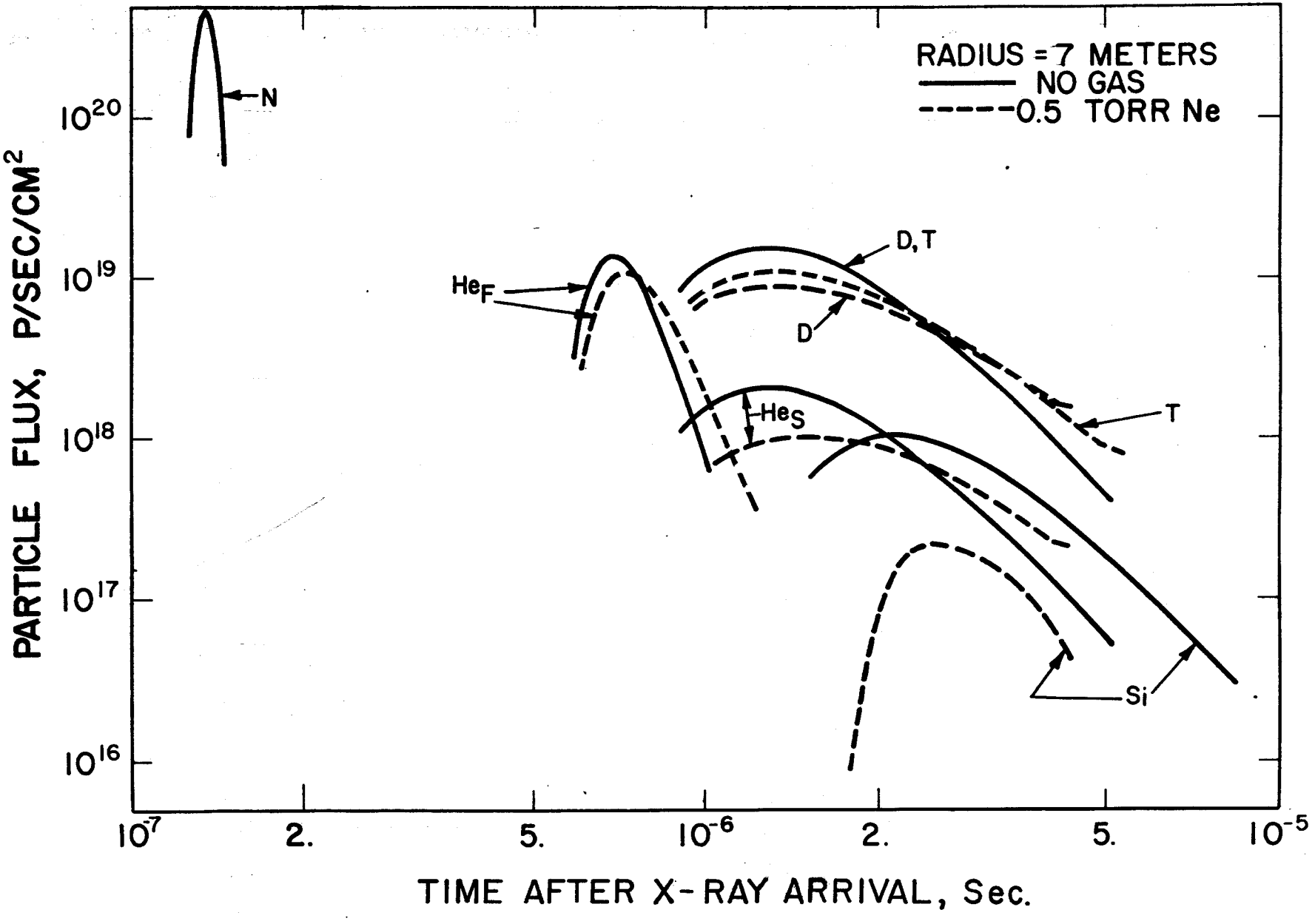

Table II

X-RAY ANALYSIS PARAMETERS

Source

Spectrum - (Blackbody Temperature, keV)

0.1 0.2 0.3 0.4 0.5 0.75 1 2 5 10

Duration (Seconds)

Impulse 10^{-12} 10^{-11} 10^{-10} 10^{-9} 10^{-8} 10^{-7}

Gas

Type

He, Ne, Xe

Pressure (at 273°K, torr)

0.1 0.5 1 5 10

Material

Stainless Steel

pressures. Only X-rays are included in this study. If there is no gas, the X-ray spectrum into the first wall is assumed to be that of a blackbody, and the energy deposition totals 1 MJ/m^2. The energy dependent absorption cross-sections of the gases used for the calculation are shown in Figure 4. Table II is a listing of the variations made in X-ray source and gas parameters for this study.

3. Energy Deposition

The total energy deposition of X-rays and ions is shown as a function of distance into the material in Figure 5. All the laser light is assumed to be absorbed in an isotropic, homogeneous, conducting media as described in reference 1. The exponential X-ray attenuation is attributed to photoelectric absorption and incoherent scattering, assuming in the calculation that no spectrum of second photons is created. Figure 6 repeats the same information with the effects of 0.5 torr Ne gas. The gas reduces the total energy deposited within the first micron by almost a factor of two, with the largest reduction coming from the heavy ion component.

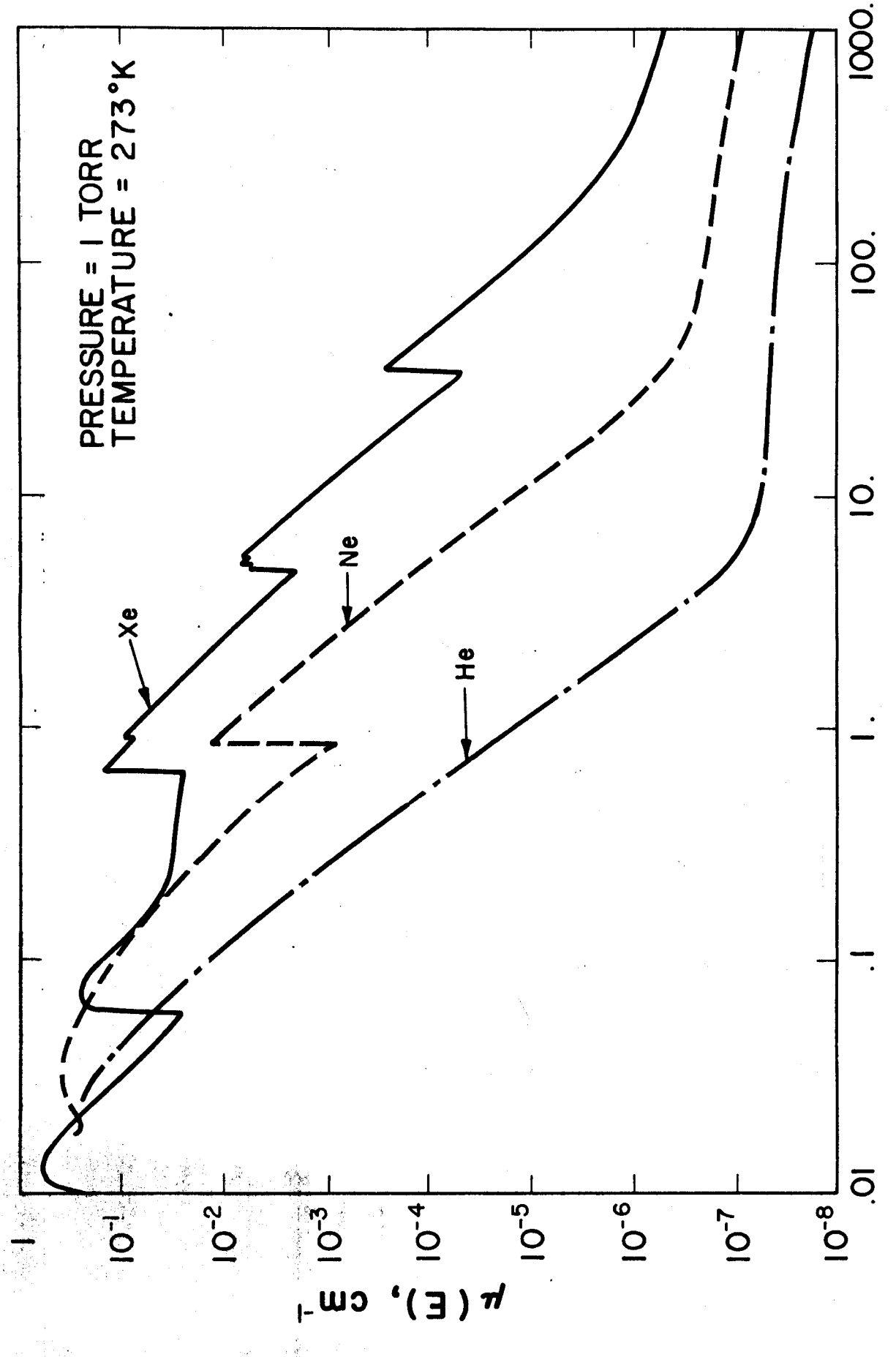
TOTAL X-RAY INTERACTION CROSS SECTIONS
PRESSURE = 1 TORR
TEMPERATURE = 273°K
Xe
Ne
He
μ (E), cm⁻¹
X-RAY ENERGY, KeV
1
10⁻¹
10⁻²
10⁻³
10⁻⁴
10⁻⁵
10⁻⁶
10⁻⁷
10⁻⁸
.01
.1
1.
10.
100.
1000.

FIGURE 4

FIGURE 5

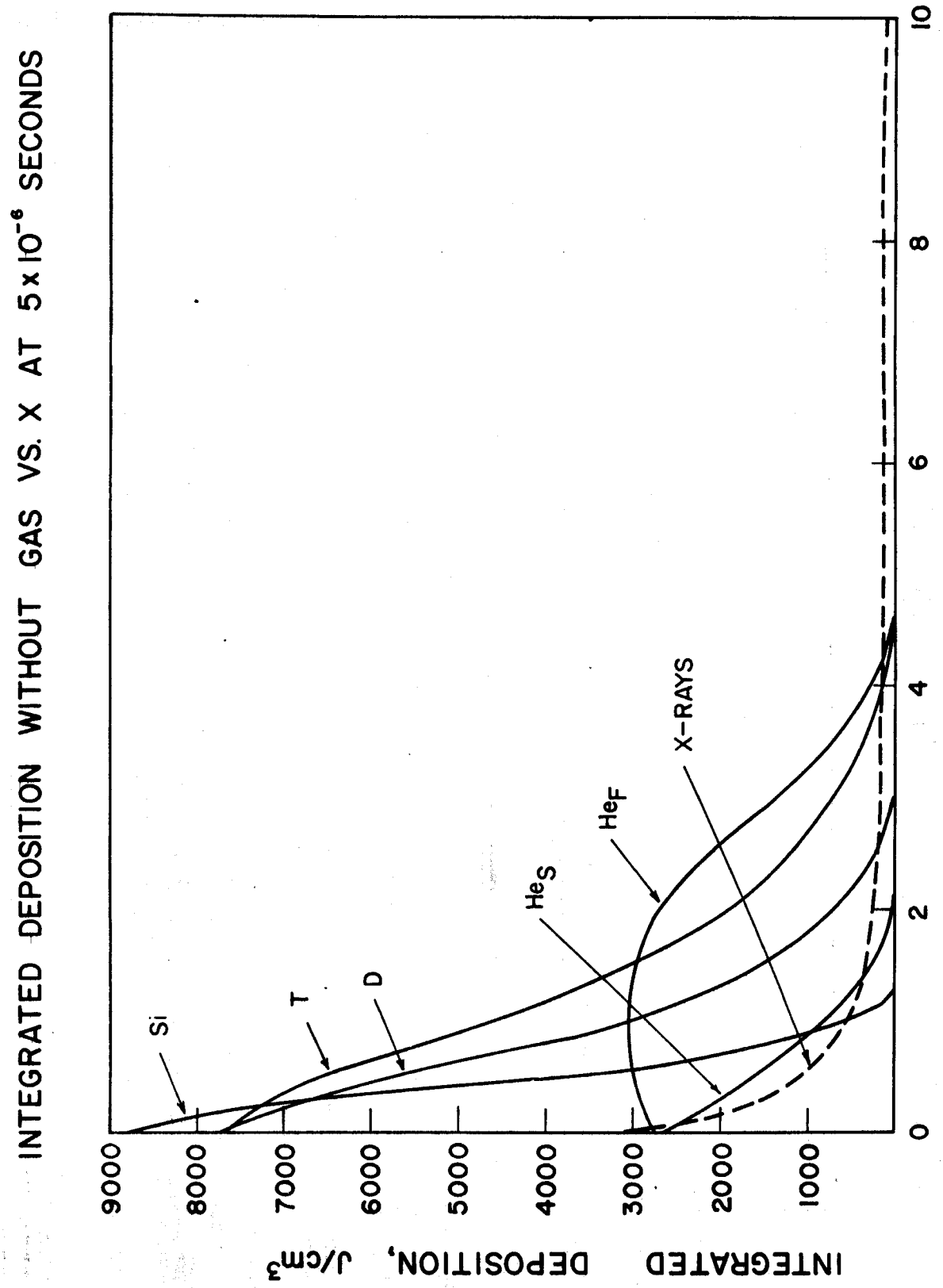
INTEGRATED DEPOSITION WITHOUT GAS VS. X AT 5 x 10⁻⁶ SECONDS
INTEGRATED DEPOSITION, J/cm³
9000
8000
7000
6000
5000
4000
3000
2000
1000
0
2
4
6
8
10
DISTANCE INTO FIRST WALL, microns
Si
T
D
He_S
He_F
X-RAYS

FIGURE 6

INTEGRATED DEPOSITION WITH GAS VS. X AT 5×10^{-6} SECONDS

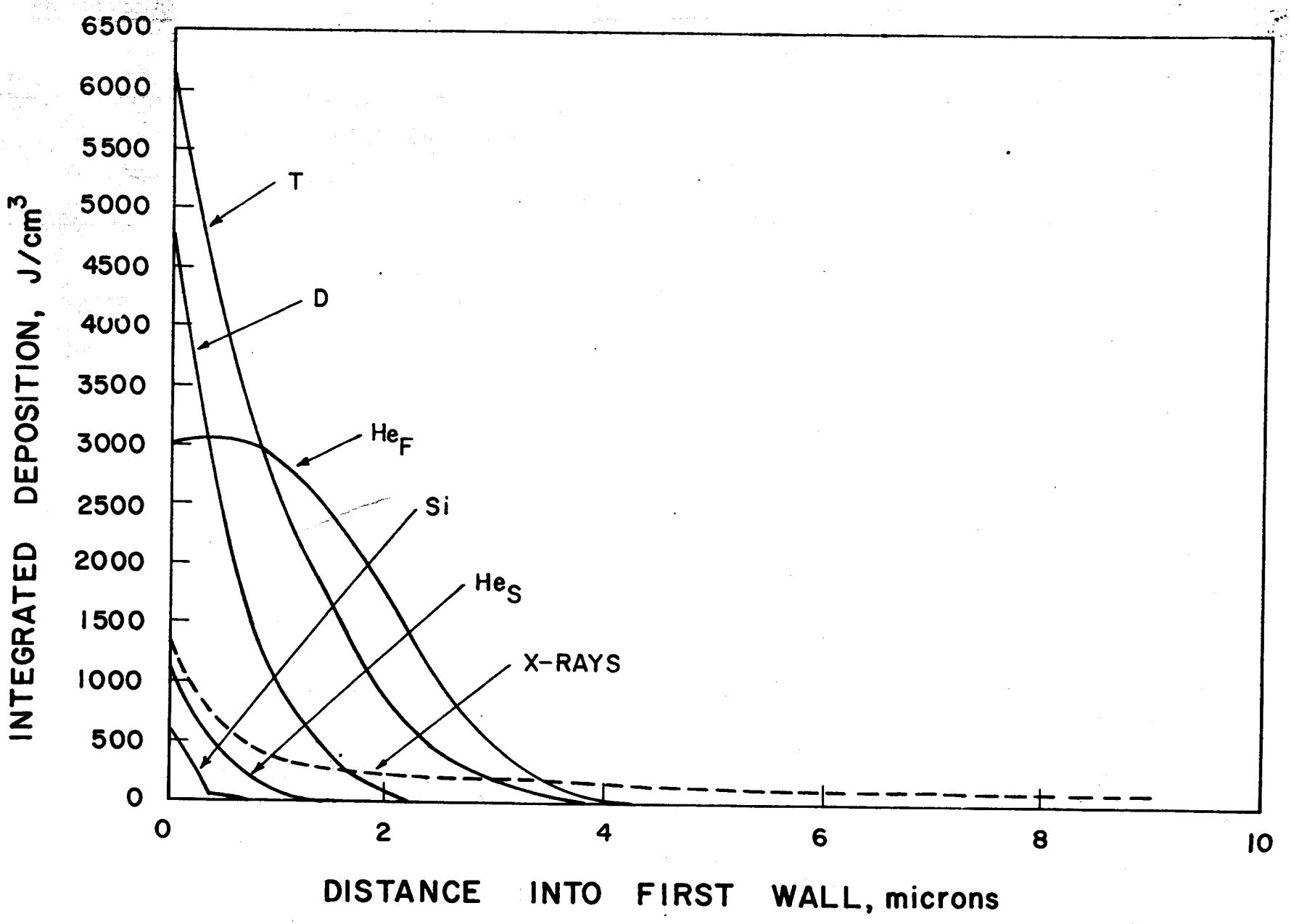

The stopping power data needed by T*DAMEN to generate energy deposition profiles were the result of a semi-empirical solution[5] to ion energy loss models formulated by Brice.[6] For $Z \leq 2$, the electronic energy loss dominates, and nuclear energy loss is negligible down to ion energies of a few keV. For such ions, T*DAMEN avoids the difficulty of obtaining spacial energy distributions from the Brice formulation by methods described in the literature.[2] For the heavier silicon ion, the inclusion of nuclear energy loss with electronic requires direct use of output from the Brice code.

The energy deposition rate and total energy deposition into the front surface (X=0) of the first wall for each ion as a function of time are given in Figures 7 and 8. There is a substantial slowing down of the ions (with the exception of fast He) due to electronic interactions in the gas, and (in the case of the heavy ions) nuclear energy deposition, which increases with ion charge and mass. Although D and T deposit the same total energy into the first wall without gas, the gas slows down the D ions more efficiently than the T ions, so their temporal depositions into the first wall are no longer superimposed after the gas is introduced.

4. Temperature Response

The solution for the spacial and temporal temperature response of an arbitrary spectrum is described in detail in references (1, 2). The response for one microexplosion will be discussed here, although the code can use LaPlace transform techniques to calculate the response after any number of pulses.

ENERGY DEPOSITION RATE

Figure 7

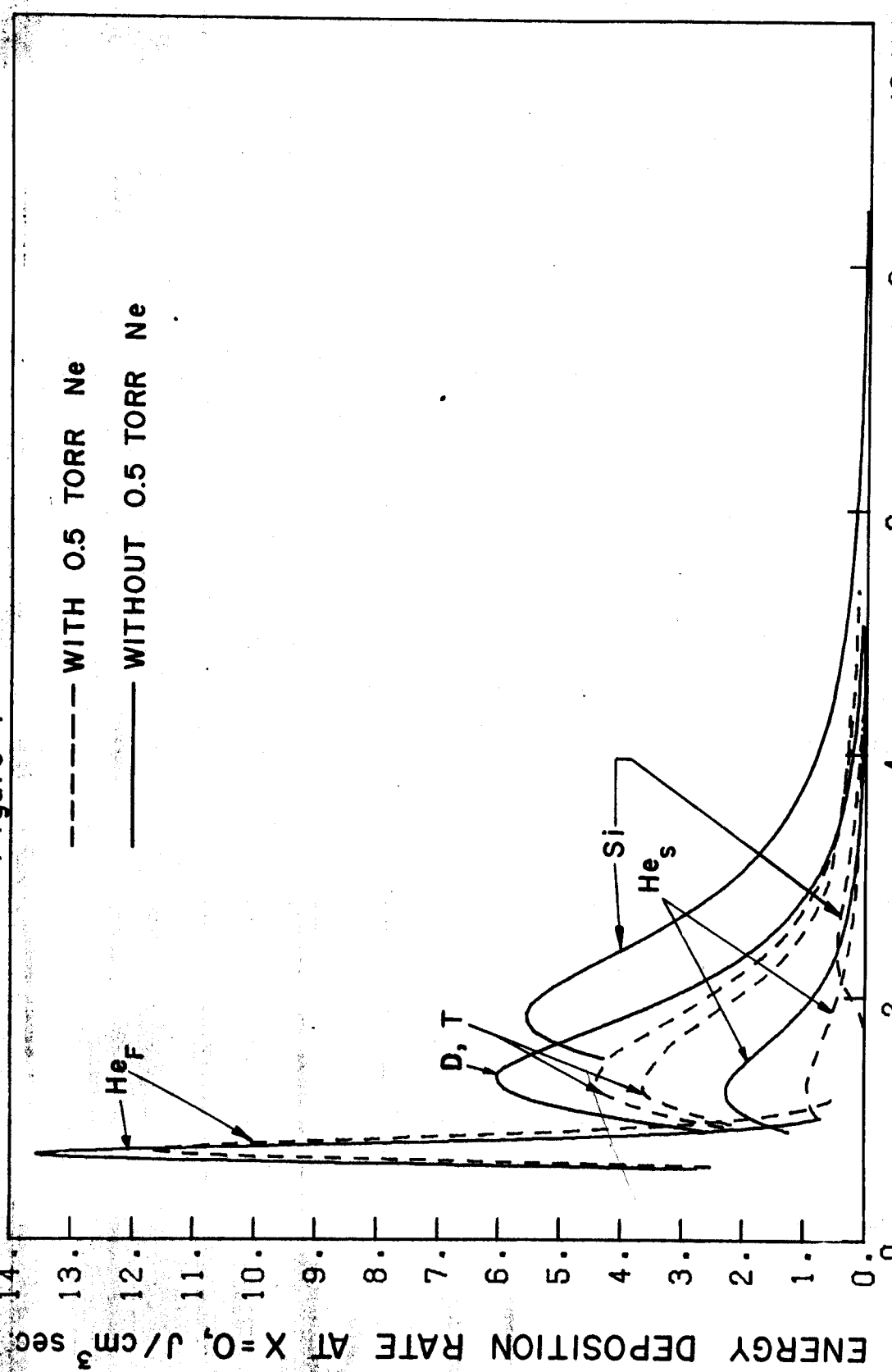

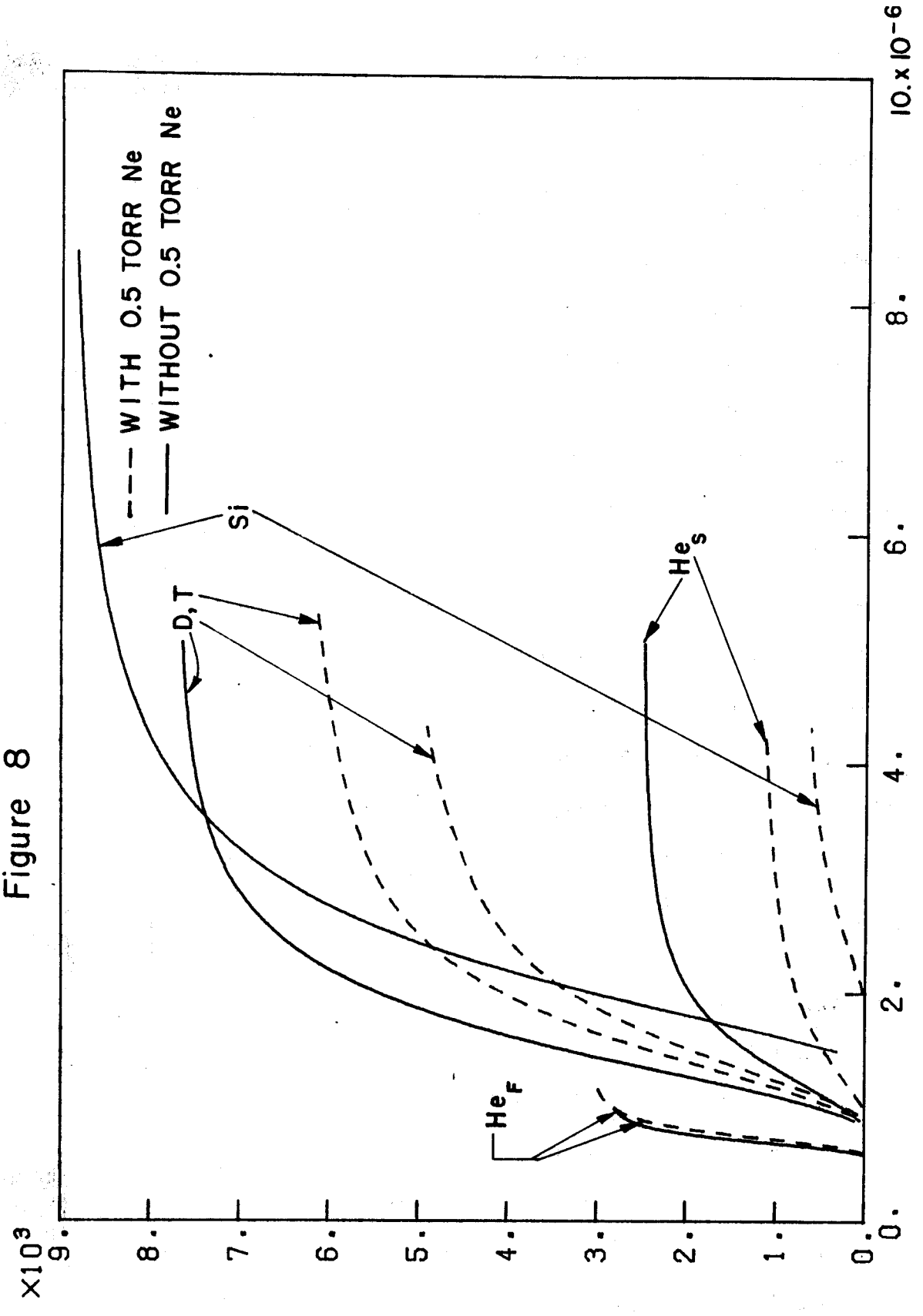
INTEGRATED ENERGY DEPOSITION
Figure 8
INTEGRATED DEPOSITION AT x = 0 , J/cm³
X10³
9.
8.
7.
6.
5.
4.
3.
2.
1.
0.
0.
2.
4.
6.
8.
10.x10⁻⁶
TIME AFTER X-RAY ARRIVAL, sec.
--- WITH 0.5 TORR Ne
— WITHOUT 0.5 TORR Ne
Si
D,T
He_S
He_F

Figure 9 shows the temperature response at the front surface (X=0) for each component of the spectrum if there is no gas. The large temperature rise picoseconds after the pellet explosion is due to X-rays (pulsewidth=10^{-9}sec) and reflected laser light. Before the heat from the photons is completely transferred away from the surface the ions arrive and deposit all their energy within 5 microns. The temperature rise from each component is not predictable by the magnitude of the total energy deposition alone. Shorter deposition times tend to increase the temperature rise and can play a more important role in the thermal response than the total energy deposited, a fact illustrated by the fast He. It is also noticed that although D and T deposit the same total energy at the same time, their temperature responses at the front surface are not identical because the energy loss rates are different at the front surface.

Figure 10 shows the temperature rise at the front surface from each component if the chamber contains 0.5 torr Ne. The decrease in magnitude of the temperature rise from each ion as compared to no gas is due mainly from the decrease in the total energy left after transit through the gas, but it is also lowered by the slightly increased deposition times.

The total temperature response at different times is plotted as a function of distance in Figure 11 for the case of no gas. After the spacial gradient from the photons is established (10^{-10}sec), the heat is quickly conducted farther into the material. After $\sim 4 \times 10^{-7}$ seconds the temperature has reached its lowest value (see Figure 9). Soon after, the ions give rise to another temperature pulse, shown in Figure 11 at

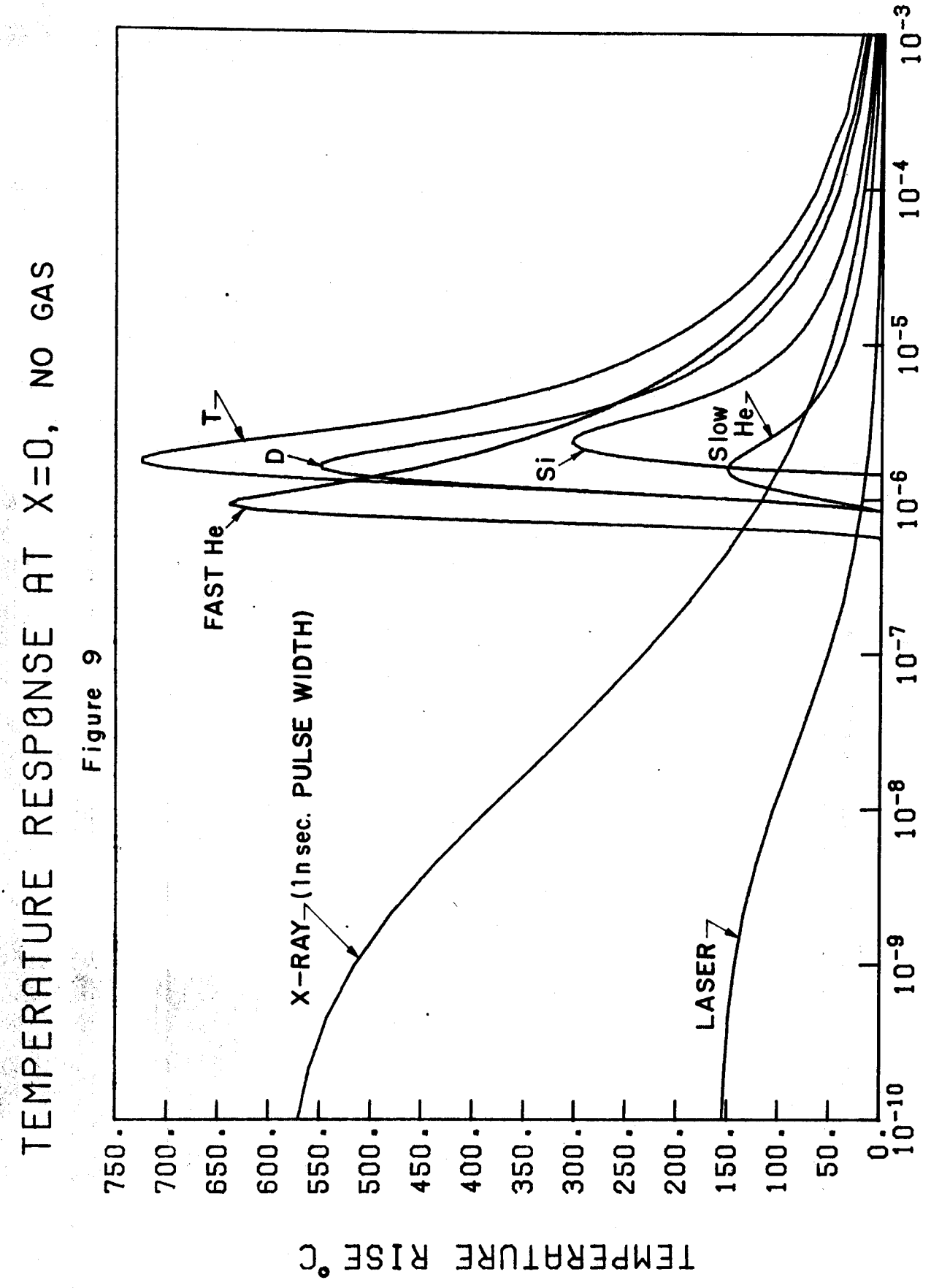
TEMPERATURE RESPONSE AT X=0, NO GAS
Figure 9
TEMPERATURE RISE °C
TIME AFTER X-RAY ARRIVAL, sec.
750.
700.
650.
600.
550.
500.
450.
400.
350.
300.
250.
200.
150.
100.
50.
0.
10^{-10}
10^{-9}
10^{-8}
10^{-7}
10^{-6}
10^{-5}
10^{-4}
10^{-3}
T
D
FAST He
Si
Slow He
X-RAY (1n sec. PULSE WIDTH)
LASER

Figure 10

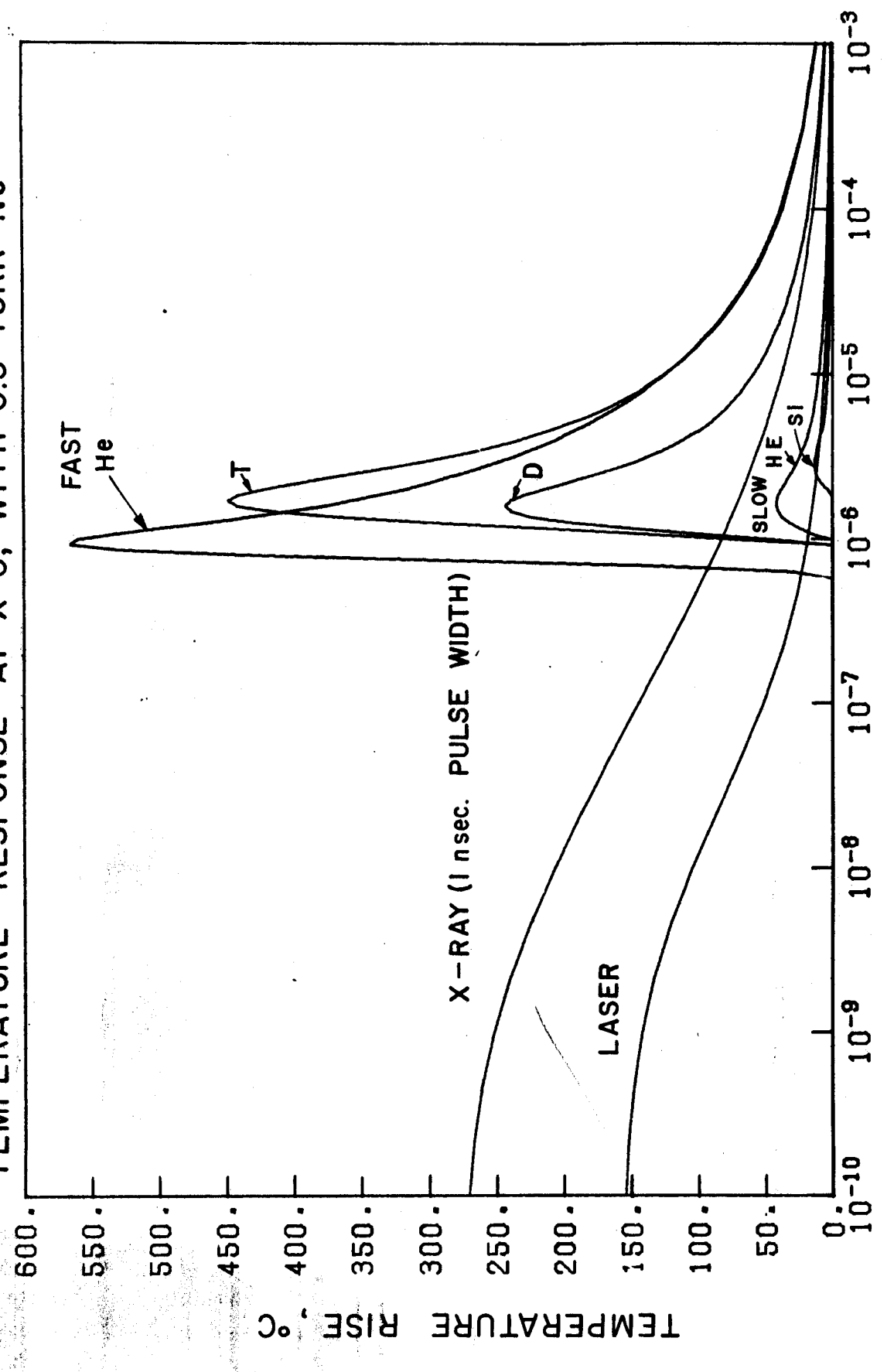
TEMPERATURE RESPONSE AT X=0, WITH 0.5 TORR Ne
FAST He
T
D
SLOW HE
SI
X-RAY (1 nsec. PULSE WIDTH)
LASER
TEMPERATURE RISE, °C
TIME AFTER X-RAY ARRIVAL, sec.
600.
550.
500.
450.
400.
350.
300.
250.
200.
150.
100.
50.
0.
10⁻¹⁰
10⁻⁹
10⁻⁸
10⁻⁷
10⁻⁶
10⁻⁵
10⁻⁴
10⁻³

FIGURE 11

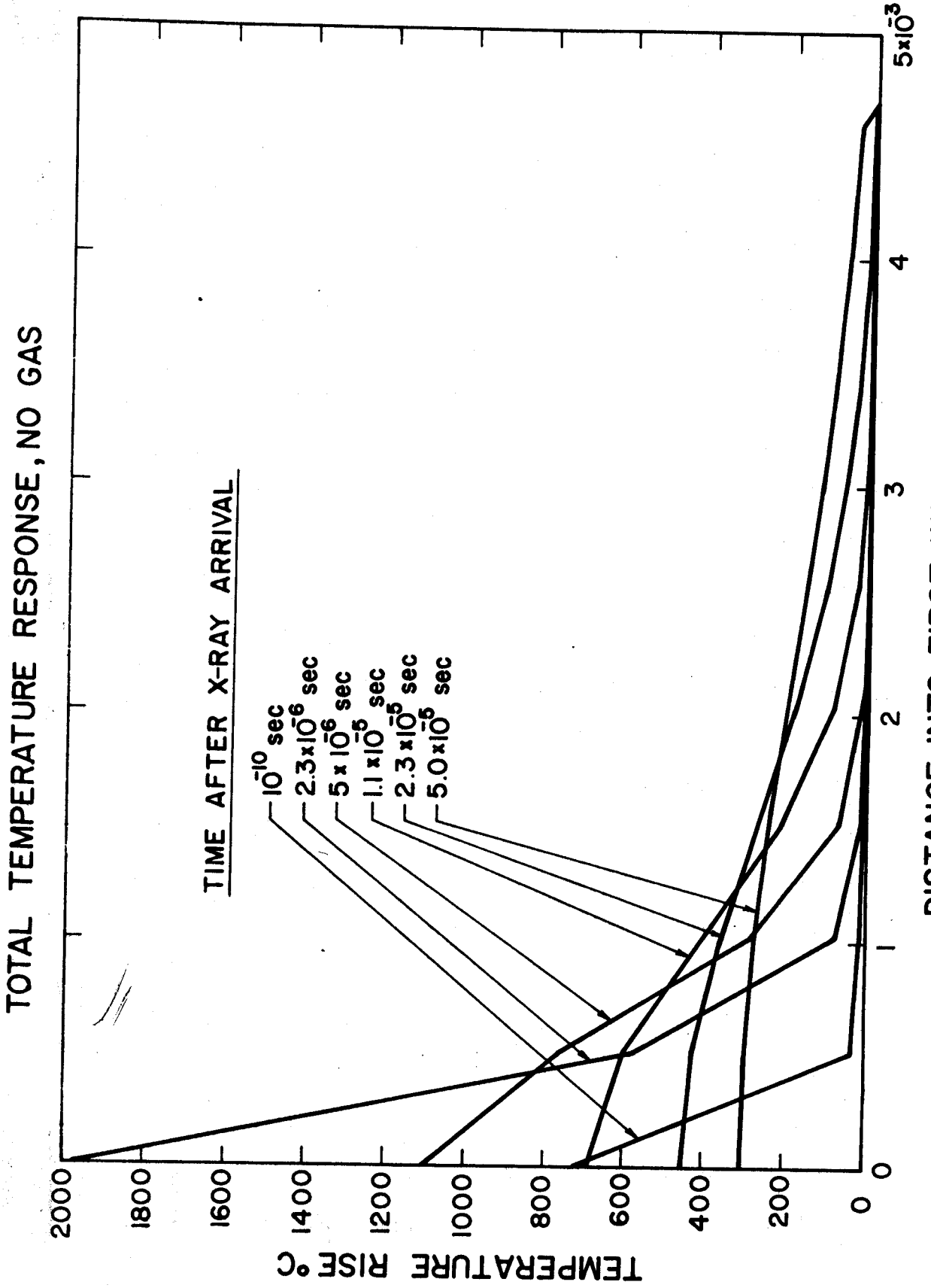
TOTAL TEMPERATURE RESPONSE, NO GAS
TIME AFTER X-RAY ARRIVAL
10^{-10} sec
2.3×10^{-6} sec
5×10^{-6} sec
1.1×10^{-5} sec
2.3×10^{-5} sec
5.0×10^{-5} sec
TEMPERATURE RISE °C
0
200
400
600
800
1000
1200
1400
1600
1800
2000
DISTANCE INTO FIRST WALL, cm
0
1
2
3
4
5×10^{-3}

2.3×10^{-6} seconds after X-ray arrival, which again decays, but over a longer time period. By the time the next pellet pulse arrives, the temperature rise should be only a few degrees above ambient.

Figure 12 illustrates the same information as Figure 11, but with the effect of having 0.5 torr Ne in the chamber. The temperature curves with and without the gas are quite similar except that the ordinates differ by a scale factor of 1/2, as illustrated in Figure 13, the total temperature rise. The temperature response from this spectrum on stainless steel with 0.5 torr neon is approximately the same as the response observed for copper with no gas layer.[3] When 0.5 torr Ne was added to the chamber for the calculation with copper, a 50% reduction in temperature response was also observed, so apparently the different thermal properties of the two materials do not influence the relative effect that 0.5 torr of neon gas has on temperature response.

5. Effects on Evaporation

Since stainless steel is a combination of different elements and current evaporation models are not sophisticated enough to make accurate predictions for such materials, the accuracy of the estimates presented here should only be considered as order of magnitude indications. The model used in this analysis to estimate the evaporation rate from the equilibrium vapor pressure is that given by Behrish.[7] The heat of sublimation of nickel, needed to relate the vapor pressure exponentially to temperature, was used since it is characteristic of the major components of stainless steels. Recondensation of surface atoms is not considered. The ambient temperature chosen was 600°C for consistency with the previous calculations.

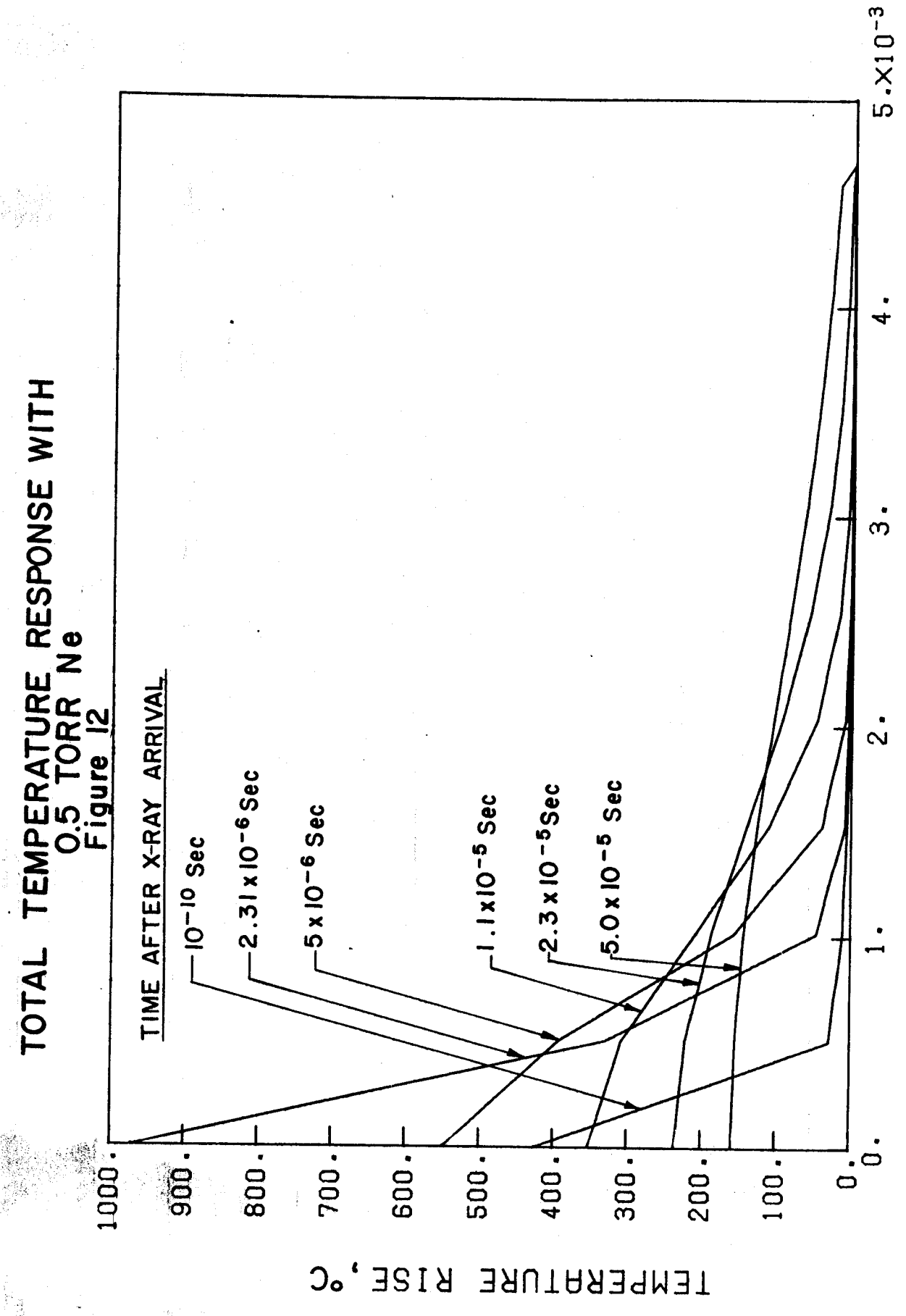
TOTAL TEMPERATURE RESPONSE WITH
0.5 TORR Ne
Figure 12
TIME AFTER X-RAY ARRIVAL
10⁻¹⁰ Sec
2.31 x 10⁻⁶ Sec
5 x 10⁻⁶ Sec
1.1 x 10⁻⁵ Sec
2.3 x 10⁻⁵ Sec
5.0 x 10⁻⁵ Sec
TEMPERATURE RISE, °C
1000.
900.
800.
700.
600.
500.
400.
300.
200.
100.
0.
0.
1.
2.
3.
4.
5.X10⁻³
DISTANCE INTO FIRST WALL, cm

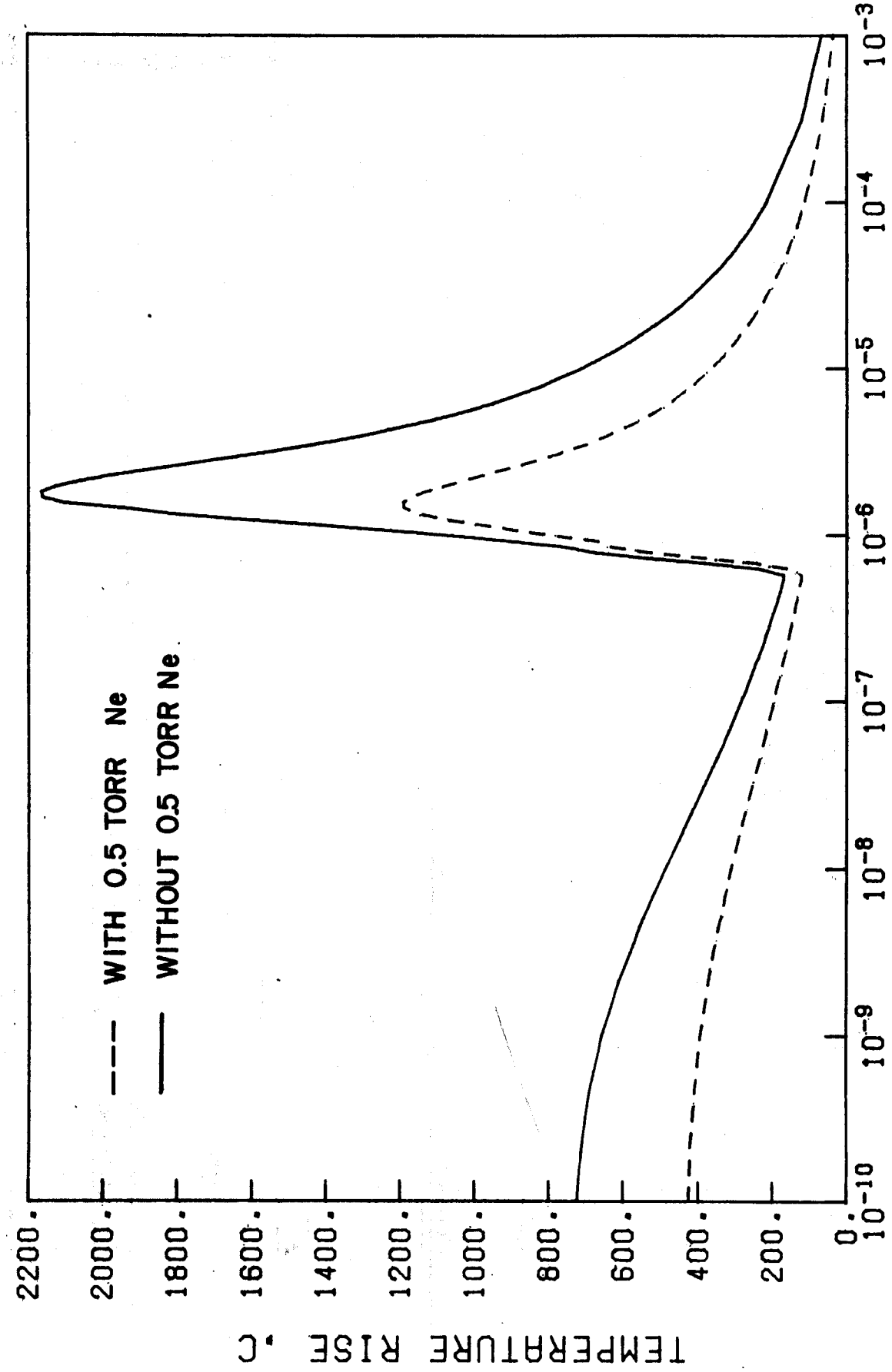
EFFECT OF CHAMBER GAS ON TEMPERATURE
WITH 0.5 TORR Ne
WITHOUT 0.5 TORR Ne
TEMPERATURE RISE °C
2200.
2000.
1800.
1600.
1400.
1200.
1000.
800.
600.
400.
200.
0.
10^{-10}
10^{-9}
10^{-8}
10^{-7}
10^{-6}
10^{-5}
10^{-4}
10^{-3}
TIME AFTER X-RAY ARRIVAL ,SEC

FIGURE 13

The magnitude of the pressure rise is described in Figure 14 for the chamber with and without .5 torr neon. The photons evaporate a negligible number of atoms during the time that they are responsible for heating and this is illustrated by the evaporation rate curves in Figure 15. This means that the large X-ray cross sections of the heavy inert gases would not be a major consideration in choosing a buffering gas from the standpoint of evaporation. Although the models used here may break down for energy deposition times smaller than the time in which a large number of lattice vibrations can occur, as is the case for photons, the qualitative conclusions about evaporation from photons should hold true.

Figure 16 shows how the number of evaporated atoms per pulse can be reduced by over four orders of magnitude with 0.5 torr neon. For the purposes of reducing evaporation and surface temperature, it is desirable to go to as high a gas pressure as possible; however, even 0.5 torr might be too large from the standpoint of laser breakdown or gas removal requirements. Then the heavier inert gases, in particular Xe, are the most promising due to their larger ion stopping powers.

6. Displacement Response

The displacement response of the spectrum used in this study has been calculated for copper by Hunter.[3] His work showed that the displacement rates in inertial confinement systems depart from the familiar radiation environments in fission and magnetic fusion devices ($\simeq 10^{-6}$ dpa/sec). To estimate the displacement response of stainless steel, stopping power input parameters for nickel were used since they are well-known and inclusion of Cr, Mn, or Fe would have relatively small effects.

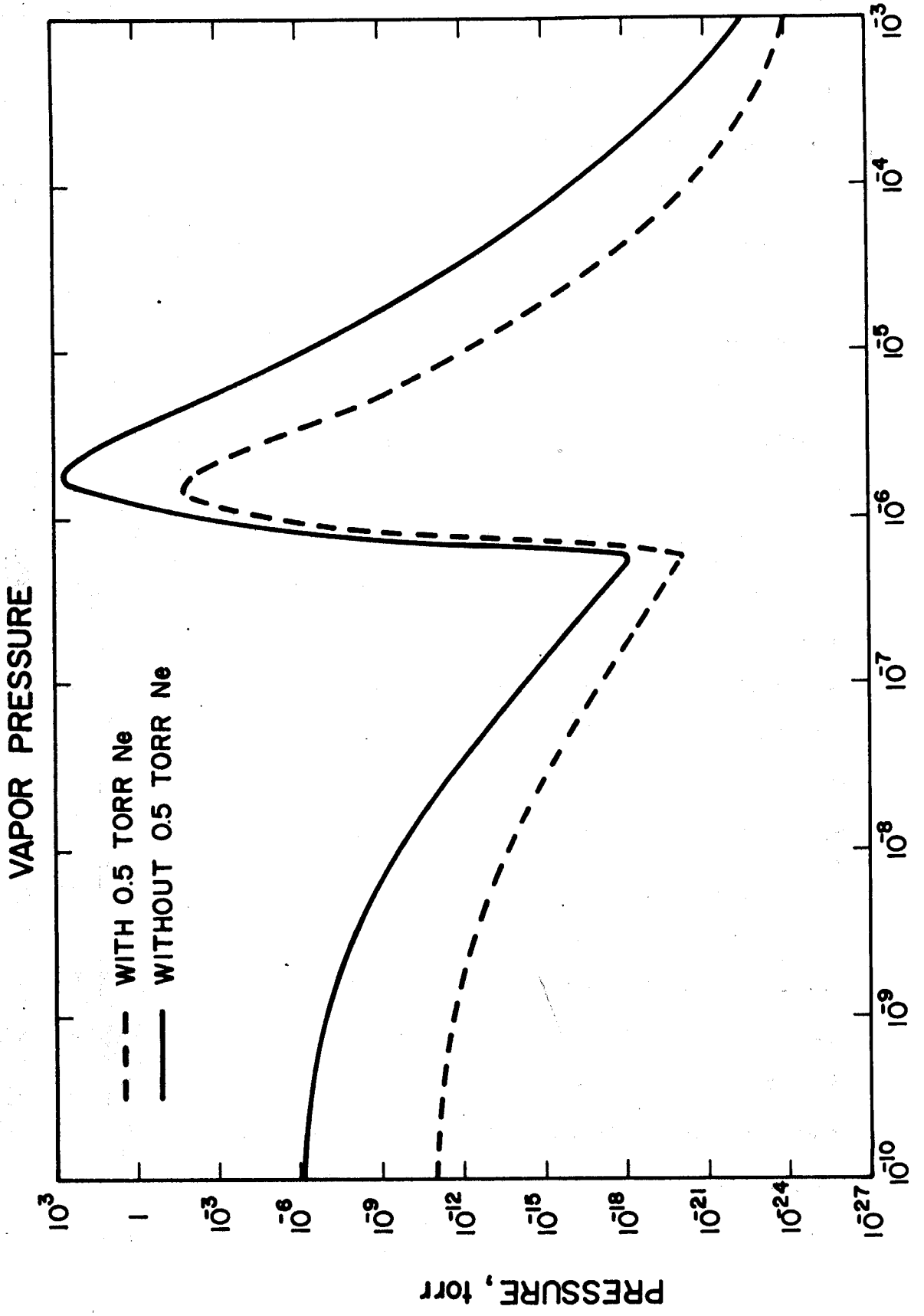
VAPOR PRESSURE
WITH 0.5 TORR Ne
WITHOUT 0.5 TORR Ne
PRESSURE, torr
TIME AFTER X-RAY ARRIVAL, sec
10^3
1
10^-3
10^-6
10^-9
10^-12
10^-15
10^-18
10^-21
10^-24
10^-27
10^-10
10^-9
10^-8
10^-7
10^-6
10^-5
10^-4
10^-3

FIGURE 14

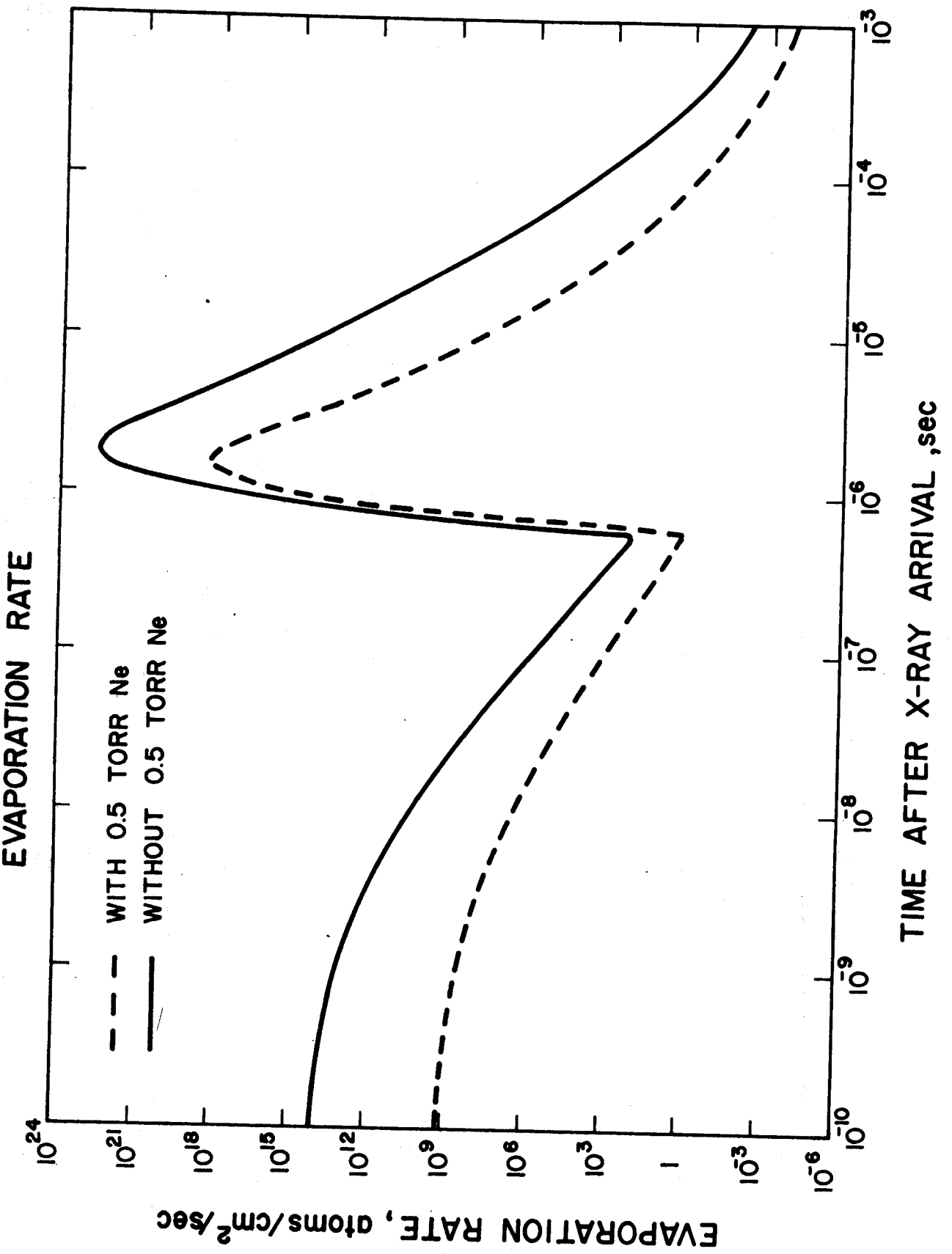
EVAPORATION RATE
WITH 0.5 TORR Ne
WITHOUT 0.5 TORR Ne
EVAPORATION RATE, atoms/cm²/sec
TIME AFTER X-RAY ARRIVAL, sec
10²⁴
10²¹
10¹⁸
10¹⁵
10¹²
10⁹
10⁶
10³
1
10⁻³
10⁻⁶
10⁻⁹
10⁻⁸
10⁻⁷
10⁻⁶
10⁻⁵
10⁻⁴
10⁻³
10⁻¹⁰

FIGURE 15

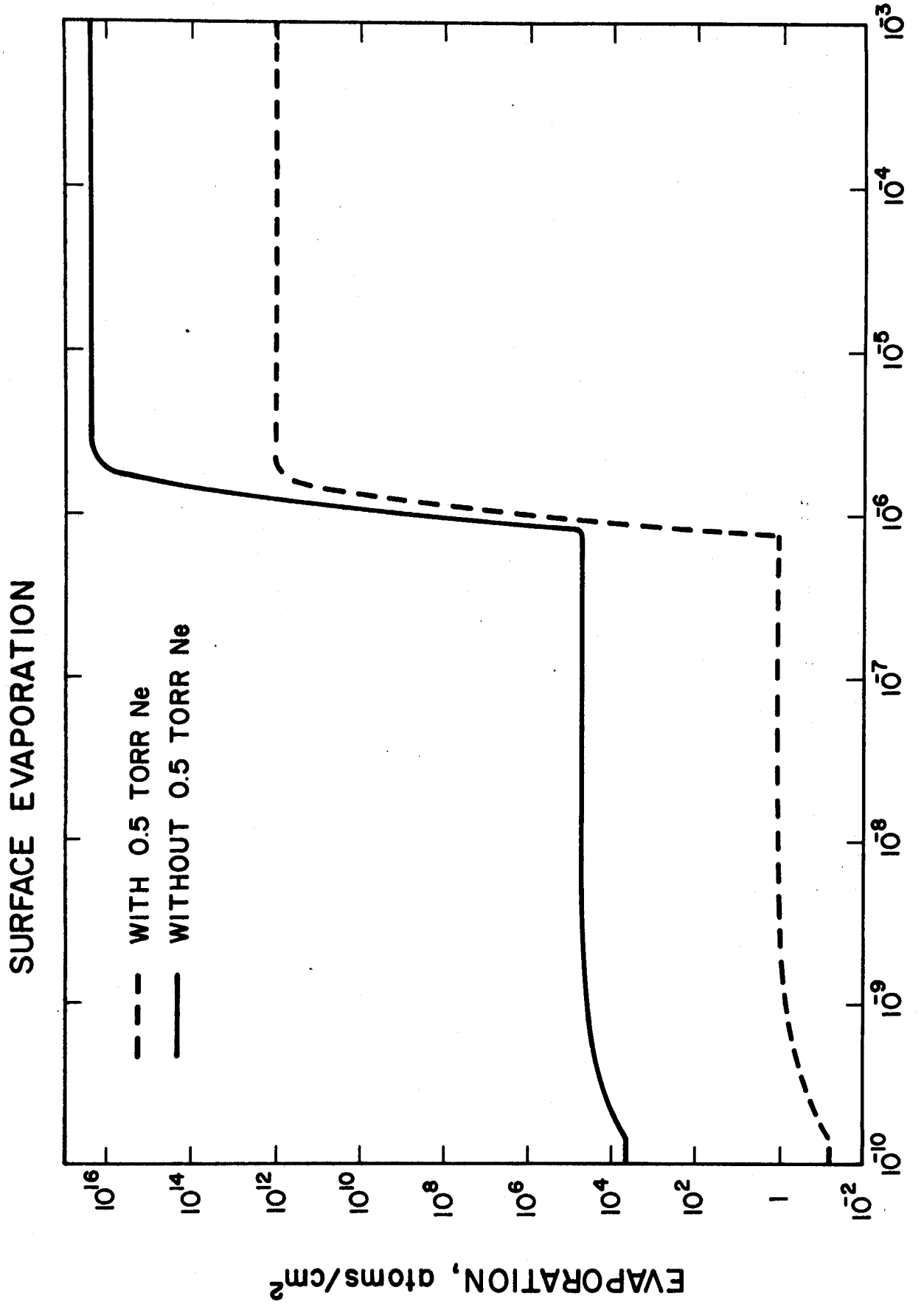
SURFACE EVAPORATION
WITH 0.5 TORR Ne
WITHOUT 0.5 TORR Ne
EVAPORATION, atoms/cm²
TIME AFTER X-RAY ARRIVAL, sec
10¹⁶
10¹⁴
10¹²
10¹⁰
10⁸
10⁶
10⁴
10²
1
10⁻²
10⁻¹⁰
10⁻⁹
10⁻⁸
10⁻⁷
10⁻⁶
10⁻⁵
10⁻⁴
10⁻³

FIGURE 16

Various input parameters for the light ions are used to provide the local displacement cross sections at any point in the material; Lindhard theory at low energies and a modified Rutherford interaction incorporating a screening function at higher energies.[8,9] For heavy ions, T*DAMEN combines the IAEA standard defect production model with a nuclear energy deposition function that is the output of an ion implantation code[6] to determine the displacement response.

The total displacement rate at the surface is plotted in Figures 17 and 18 (without and with 0.5 torr neon, respectively) to show the relationship of the displacement spike from the ions with the temperature spike. The superposition of these spikes in time is known to affect the point cluster defect behavior. It can be seen from the figures that although the magnitudes of the damage rate and temperature response are both reduced by 50% with the presence of 0.5 torr neon, the relationship of the peaks to each other is not significantly altered. The time integrated surface dpa is graphically illustrated in Figure 19, with and without the gas.

The 0.5 torr of neon has a larger affect on displacement response farther into the first wall, as seen in Figure 20. Not only is the magnitude significantly reduced everywhere in the first wall, but the total dpa peak position is shifted closer toward the surface. This is mainly due to the heavy ions, which give rise to a large percentage of the displacement peak. The silicon energy spectrum is reduced (see Figure 3) and the end-of-range for the heavy ions, where the nuclear damage occurs, is closer to the surface.

Figures 21 through 23 show the dpa rate contributions of each component at three different distances into the material as a function of arrival

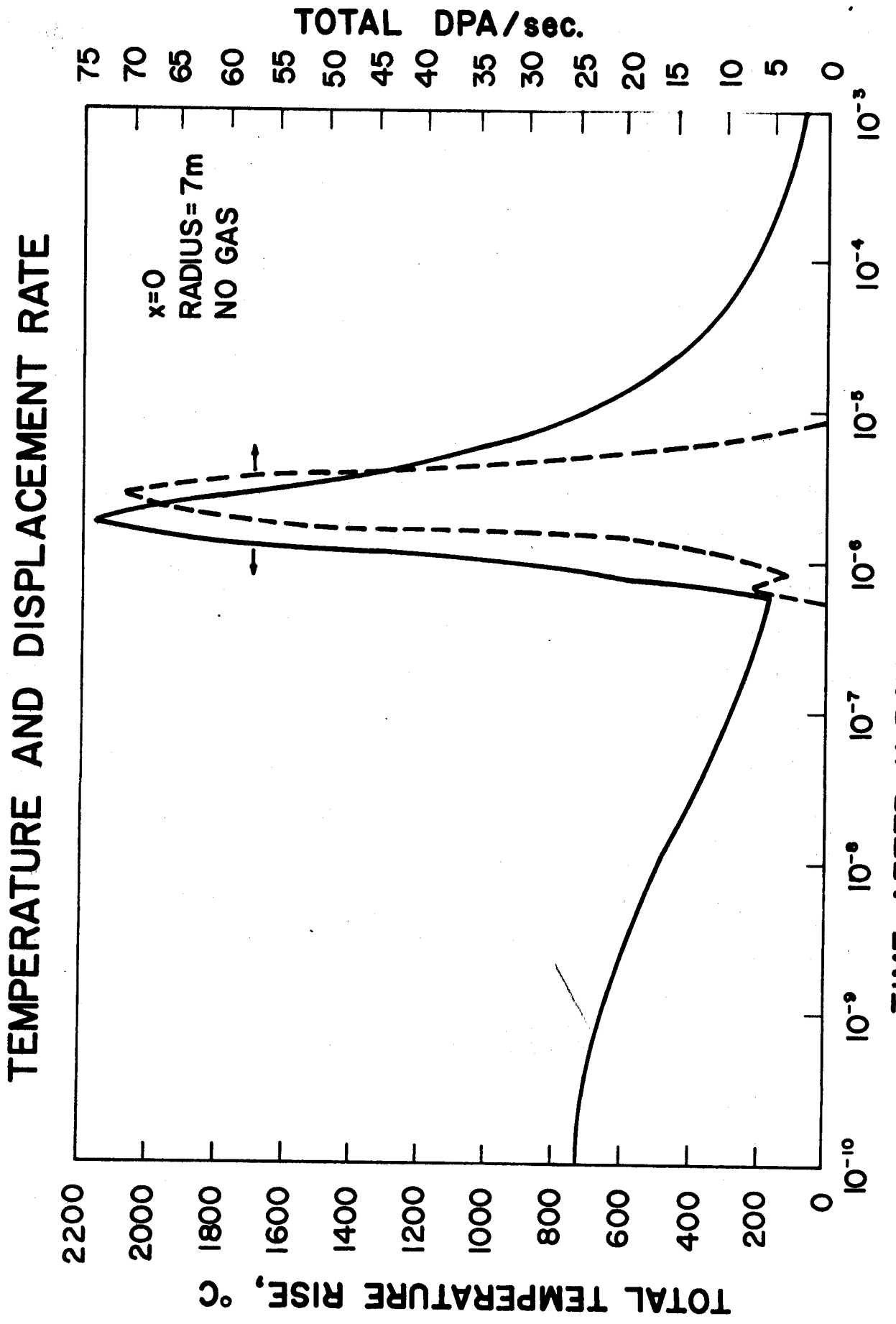
TEMPERATURE AND DISPLACEMENT RATE
TOTAL DPA/sec.
75 70 65 60 55 50 45 40 35 30 25 20 15 10 5 0
x=0
RADIUS=7m
NO GAS
TOTAL TEMPERATURE RISE, °C
2200 2000 1800 1600 1400 1200 1000 800 600 400 200 0
TIME AFTER X-RAY ARRIVAL, seconds
10^{-10} 10^{-9} 10^{-8} 10^{-7} 10^{-6} 10^{-5} 10^{-4} 10^{-3}

FIGURE 17

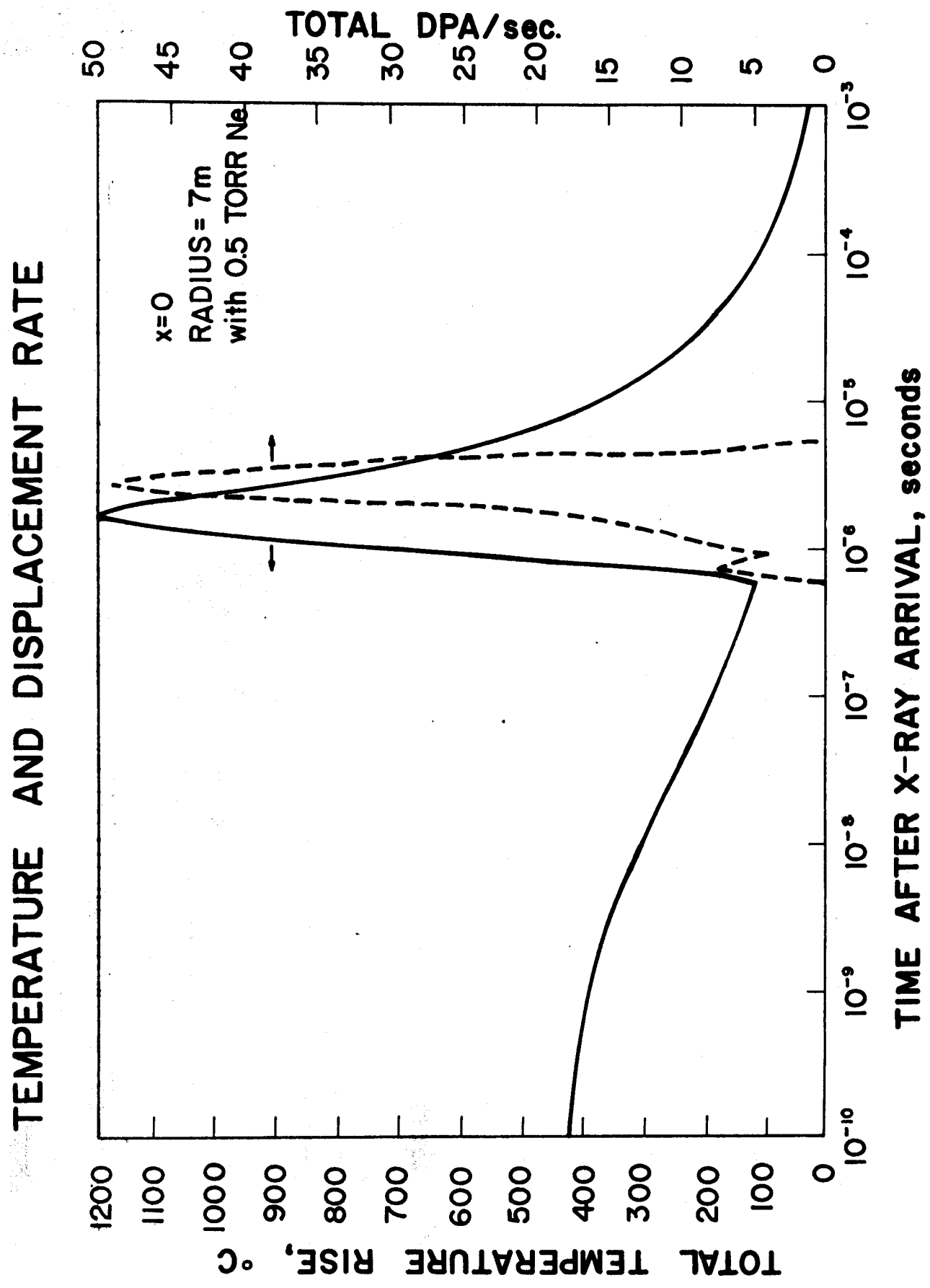
TEMPERATURE AND DISPLACEMENT RATE
TOTAL DPA/sec.
50
45
40
35
30
25
20
15
10
5
0
x=0
RADIUS= 7m
with 0.5 TORR Ne
TOTAL TEMPERATURE RISE, °C
1200
1100
1000
900
800
700
600
500
400
300
200
100
0
10^{-10}
10^{-9}
10^{-8}
10^{-7}
10^{-6}
10^{-5}
10^{-4}
10^{-3}
TIME AFTER X-RAY ARRIVAL, seconds

FIGURE 18

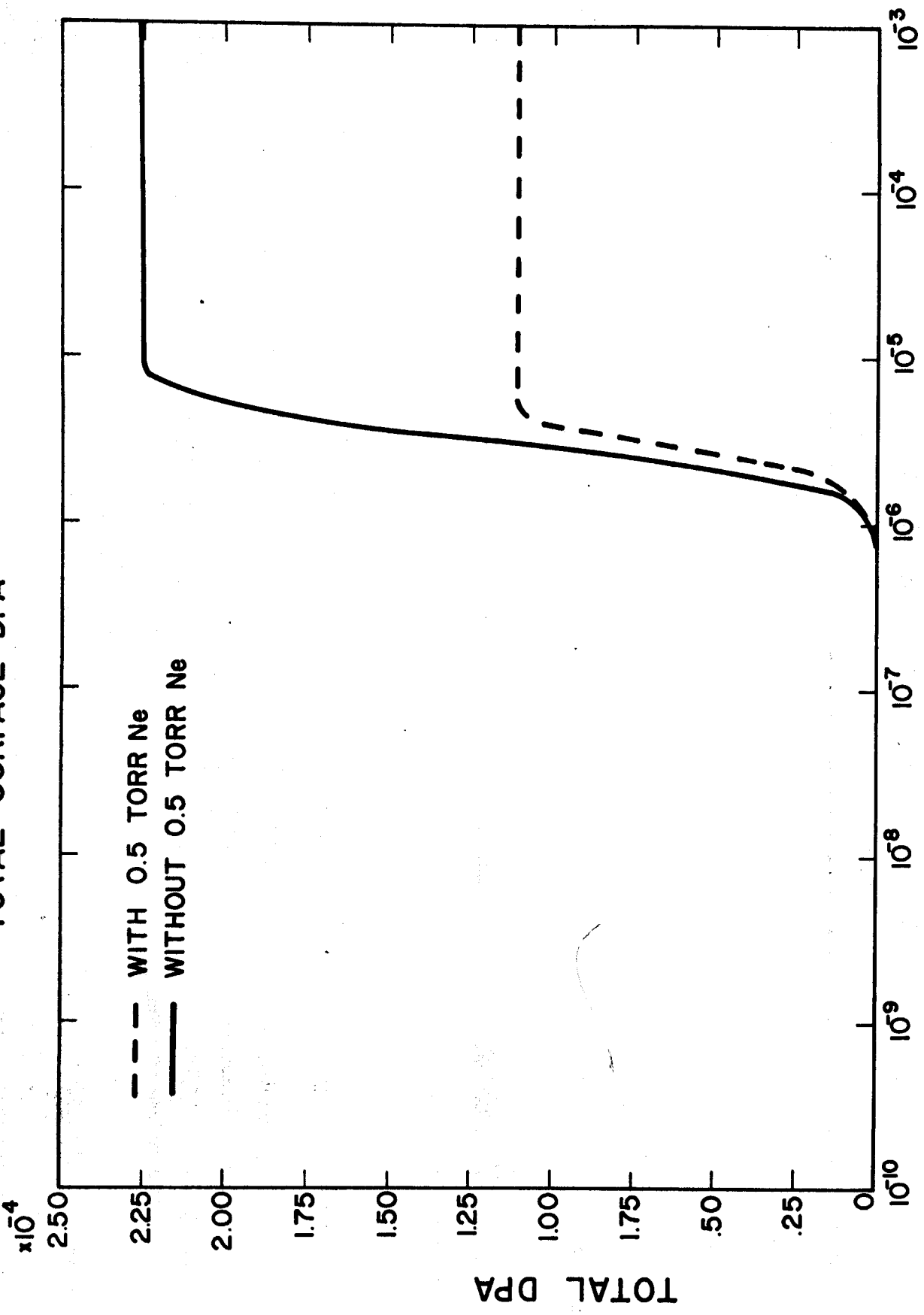
TOTAL SURFACE DPA
WITH 0.5 TORR Ne
WITHOUT 0.5 TORR Ne
TOTAL DPA
x10⁻⁴
2.50
2.25
2.00
1.75
1.50
1.25
1.00
.75
.50
.25
0
10⁻¹⁰
10⁻⁹
10⁻⁸
10⁻⁷
10⁻⁶
10⁻⁵
10⁻⁴
10⁻³
TIME AFTER X-RAY ARRIVAL, sec

FIGURE 19

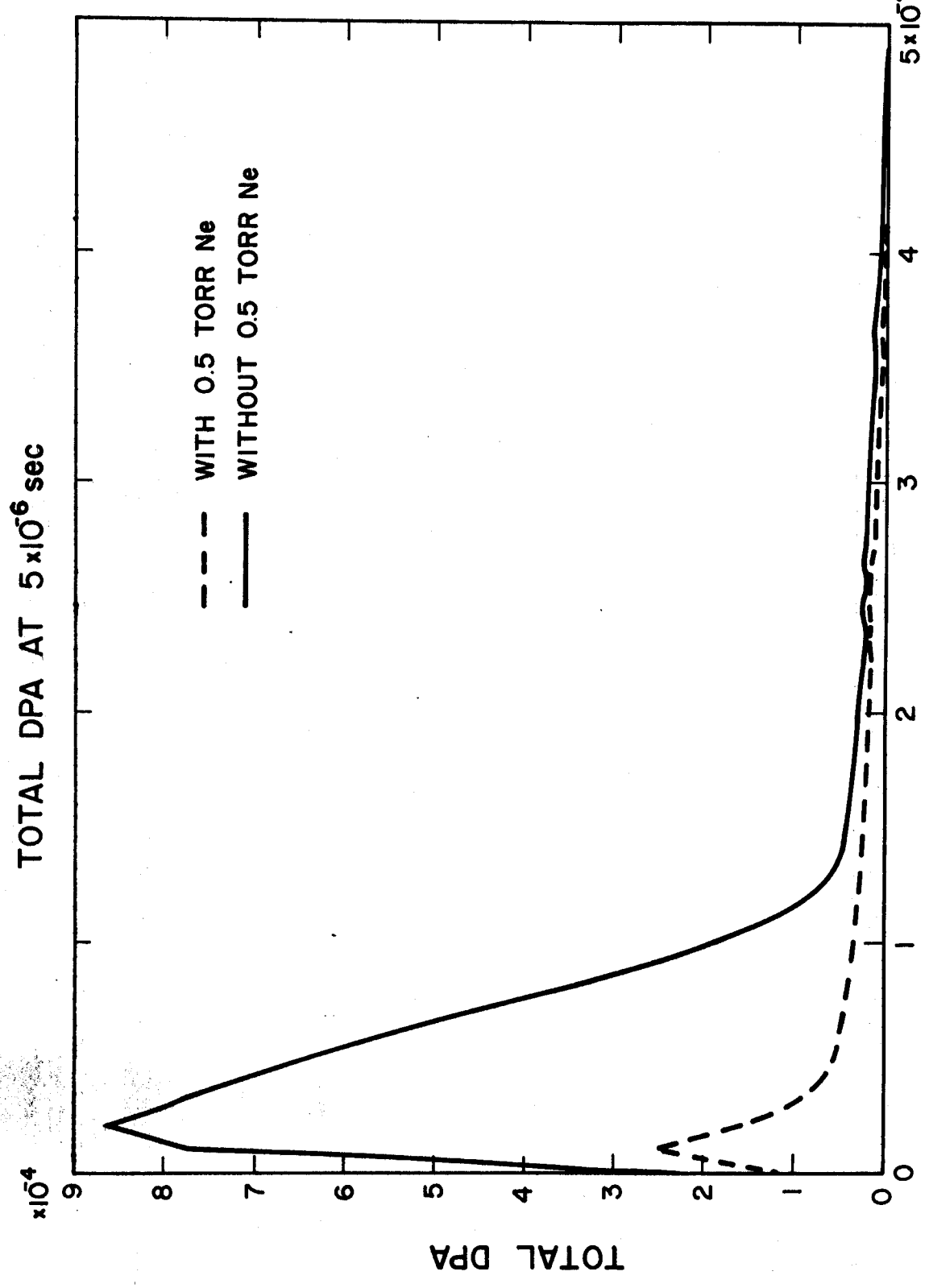
TOTAL DPA AT 5x10⁻⁶ sec
WITH 0.5 TORR Ne
WITHOUT 0.5 TORR Ne
TOTAL DPA
x10⁻⁴
0
1
2
3
4
5
6
7
8
9
DISTANCE INTO FIRST WALL, cm
0
1
2
3
4
5x10⁻⁴

FIGURE 20

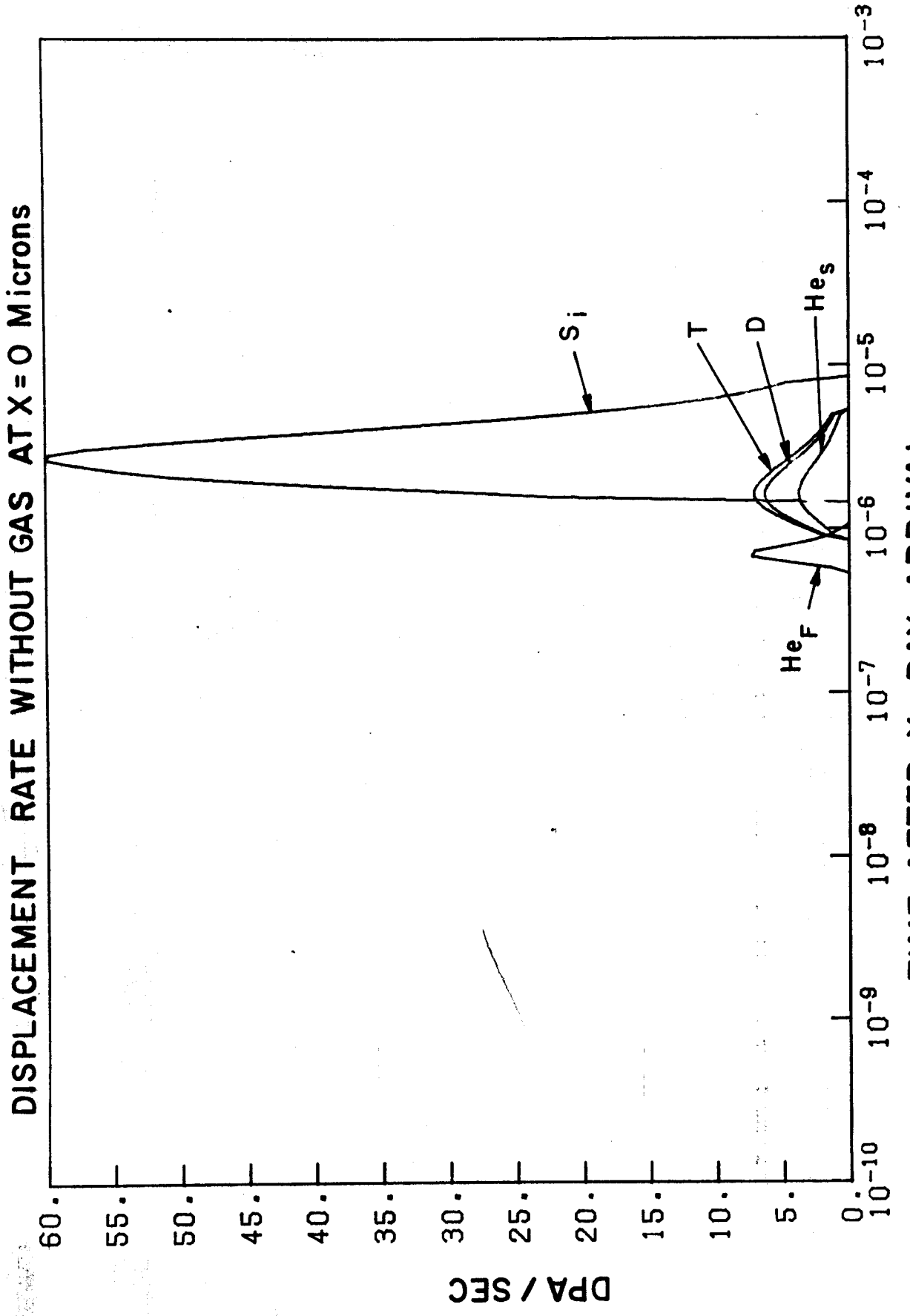
DISPLACEMENT RATE WITHOUT GAS AT X = 0 Microns
DPA / SEC
60.
55.
50.
45.
40.
35.
30.
25.
20.
15.
10.
5.
0.
10^{-10}
10^{-9}
10^{-8}
10^{-7}
10^{-6}
10^{-5}
10^{-4}
10^{-3}
TIME AFTER X-RAY ARRIVAL, sec
Si_i
T
D
He_S
He_F

FIGURE 21

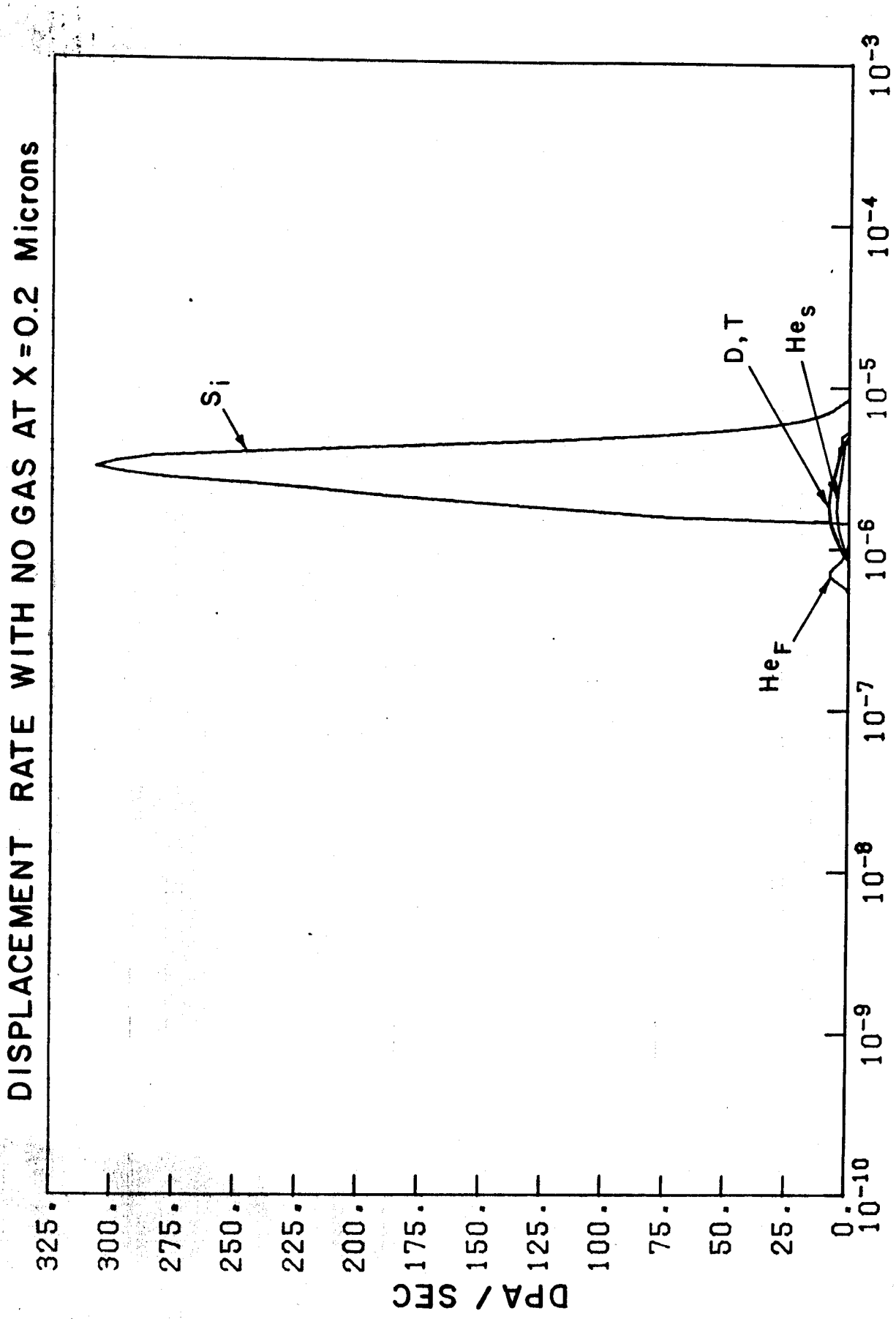
DISPLACEMENT RATE WITH NO GAS AT X=0.2 Microns
DPA / SEC
TIME AFTER X-RAY ARRIVAL, sec
S_i
D,T
He_S
He_F
325.
300.
275.
250.
225.
200.
175.
150.
125.
100.
75.
50.
25.
0.
10^{-10}
10^{-9}
10^{-8}
10^{-7}
10^{-6}
10^{-5}
10^{-4}
10^{-3}

FIGURE 22

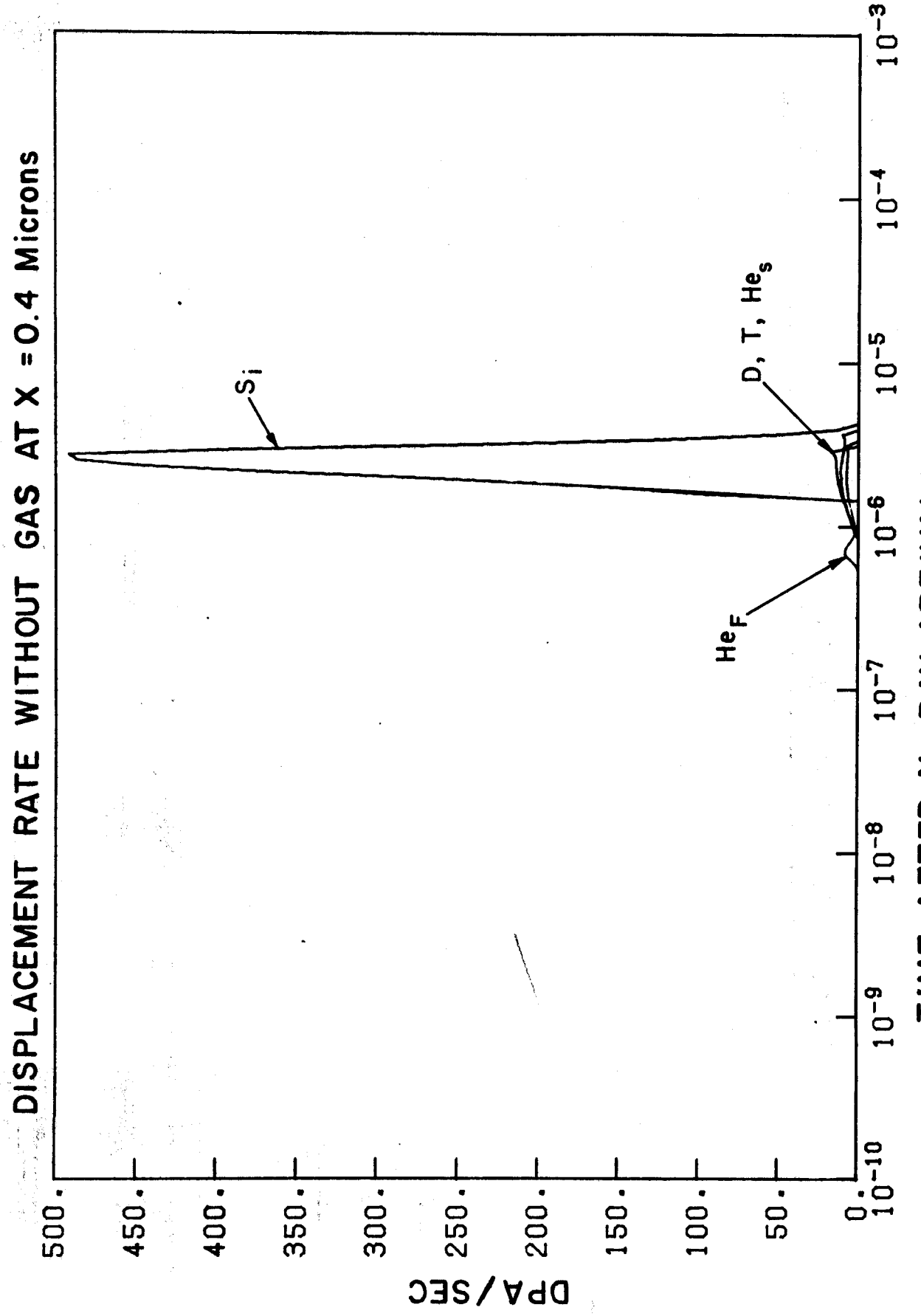
DISPLACEMENT RATE WITHOUT GAS AT X =0.4 Microns
DPA/SEC
500.
450.
400.
350.
300.
250.
200.
150.
100.
50.
0.
10^{-10}
10^{-9}
10^{-8}
10^{-7}
10^{-6}
10^{-5}
10^{-4}
10^{-3}
TIME AFTER X-RAY ARRIVAL, sec
Si_i
D, T, He_s
He_F

FIGURE 23

time (after X-rays), and illustrate the significant contributions of the heavy ion component. At X=.4 microns the total dpa rate is near its maximum for the case of no gas. Figures 24 through 26 then illustrate how each ion's contribution to the dpa rate is reduced by 0.5 torr of neon. The fast helium ions are particularly unaffected, as indicated by the small change in its energy spectrum (Figure 3).

7. Parametric Analysis of X-ray Response

The parameter study presented here examines the response of stainless steel to variations in X-ray spectra and gas parameters. The parameters chosen for the analysis were given in Table II, and the results are presented in tabular and graphical form.

All calculations for the temperature response were performed at the surface of the first wall using a spherical cavity of 2.82 meter radius and 1 MJ of X-ray output. The results can be expressed as a temperature rise (ΔT in this paper) per cm^2 per Joule of X-ray energy reaching the first wall in the absence of gas so that extrapolation to other geometries can be made. Care must be used when considering a gas layer because the final X-ray spectrum that appears at the first wall is different than that originally emitted (especially at the low energy end). The data for the graphs are presented in Tables III to V. Each table contains the variations in gas pressure, source time, and blackbody temperature for a particular gas.

The effect of gas pressure for the three different gases He, Ne, and Xe on the surface temperature response of stainless steel is shown in Figures 27 through 29 for a source duration of 10^{-9} seconds. Figures 30 through 32 illustrate the results of the same calculation for a longer source duration 10^{-7} seconds. The temperature response for helium at 0.1 torr is essentially the same as for the response with no gas when the source duration is 10^{-9} seconds.

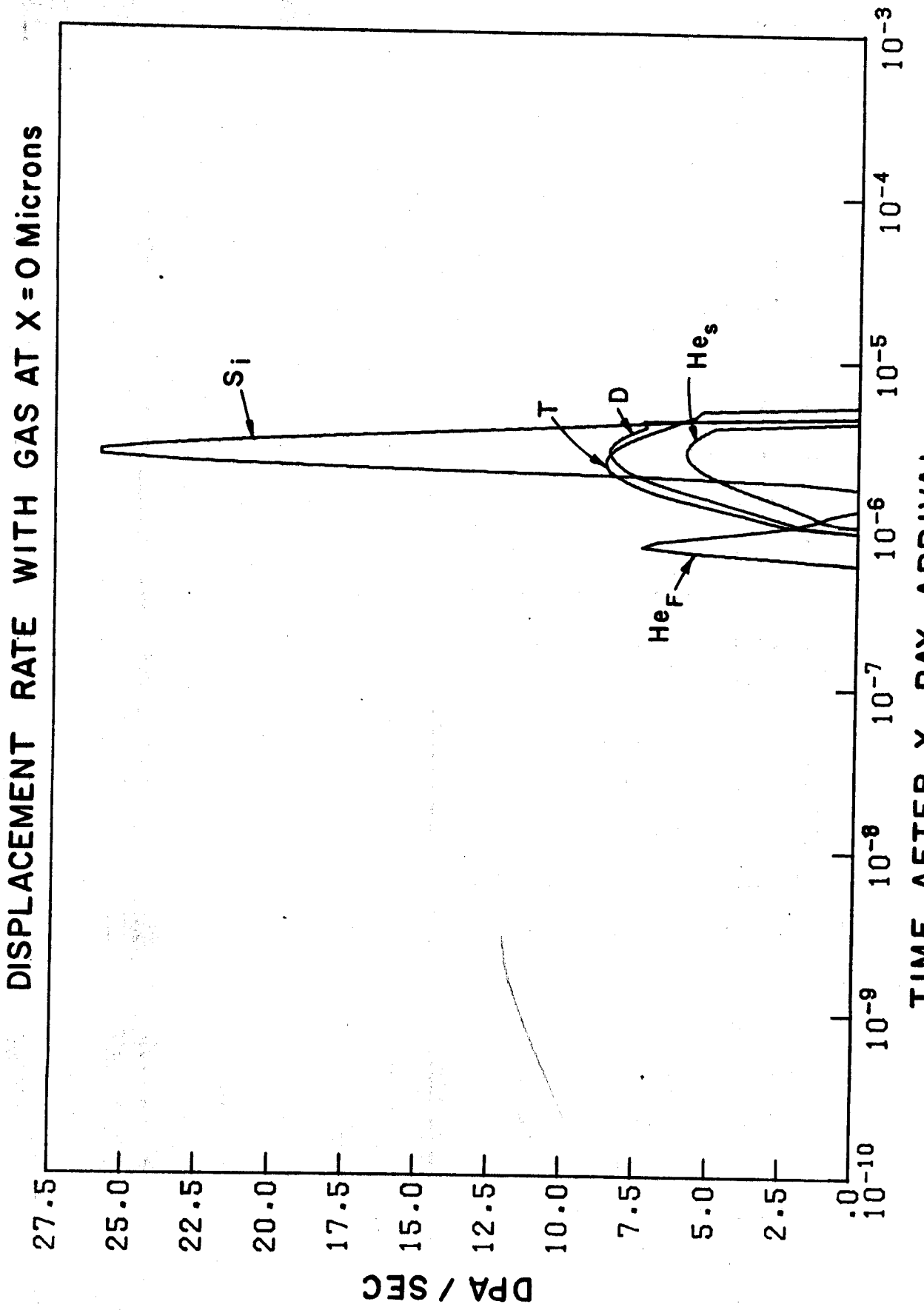
DISPLACEMENT RATE WITH GAS AT X = 0 Microns
DPA / SEC
27.5
25.0
22.5
20.0
17.5
15.0
12.5
10.0
7.5
5.0
2.5
.0
Si
T
D
He_S
He_F
10^-10
10^-9
10^-8
10^-7
10^-6
10^-5
10^-4
10^-3
TIME AFTER X-RAY ARRIVAL, sec

FIGURE 24

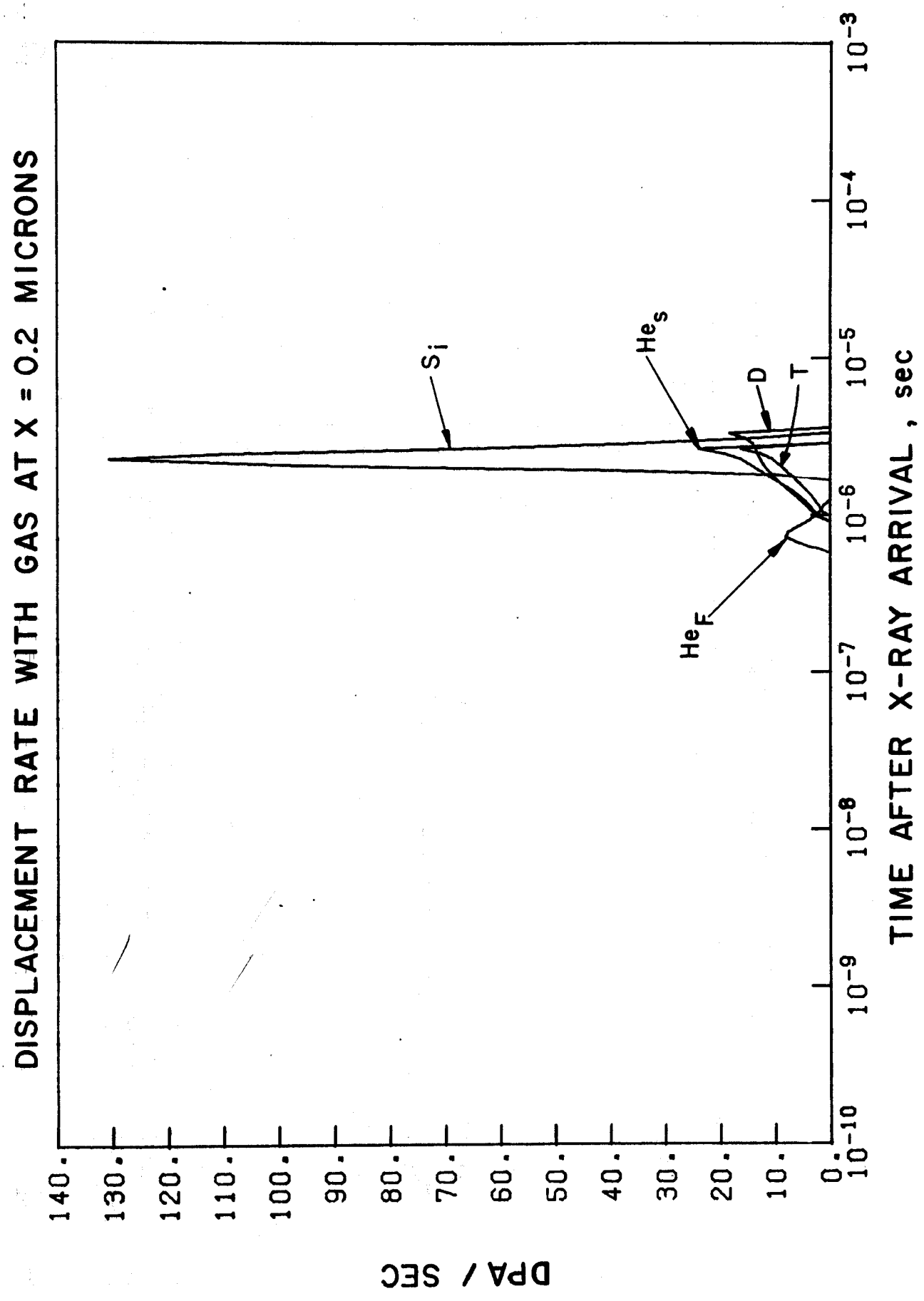
DISPLACEMENT RATE WITH GAS AT X = 0.2 MICRONS
DPA / SEC
140.
130.
120.
110.
100.
90.
80.
70.
60.
50.
40.
30.
20.
10.
0.
10^{-10}
10^{-9}
10^{-8}
10^{-7}
10^{-6}
10^{-5}
10^{-4}
10^{-3}
TIME AFTER X-RAY ARRIVAL , sec
Si_i
He_s
D
T
He_F

FIGURE 25

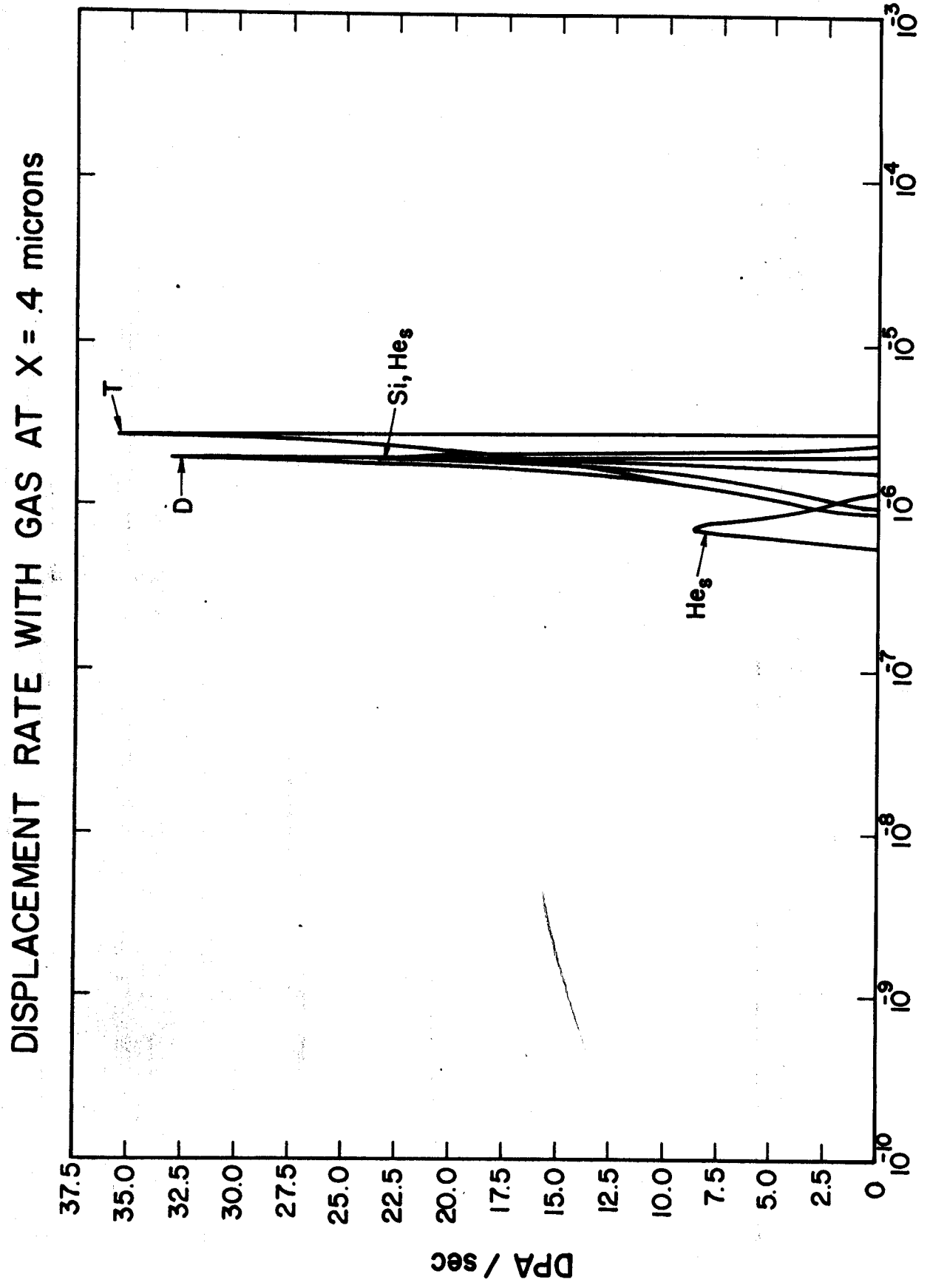
DISPLACEMENT RATE WITH GAS AT X = .4 microns
DPA / sec
TIME AFTER X-RAY ARRIVAL , sec
T
D
Si, He$_s$
He$_s$
37.5
35.0
32.5
30.0
27.5
25.0
22.5
20.0
17.5
15.0
12.5
10.0
7.5
5.0
2.5
0
10^{-3}
10^{-4}
10^{-5}
10^{-6}
10^{-7}
10^{-8}
10^{-9}
10^{-10}

FIGURE 26

TABLE III: NORMALIZED THERMAL RESPONSE FROM X-RAYS IN STAINLESS STEEL WITH HELIUM GAS PROTECTION

logΔt (sec)	BLACKBODY TEMPERATURE (KEV)									
	.1	.2	.3	.4	.5	.75	1.	2.	5.	10.
	TORR=.1									
-12	.193+5	.136+5	.109+5	.838+4	.655+4	.340+4	.215+4	.640+3	.164+3	.420+2
-11	.178+5	.129+5	.105+5	.810+4	.634+4	.332+4	.210+4	.633+3	.163+3	.419+2
-10	.153+5	.118+5	.971+4	.756+4	.595+4	.316+4	.201+4	.620+3	.161+3	.418+2
-9	.111+5	.929+4	.791+4	.630+4	.502+4	.277+4	.179+4	.586+3	.157+3	.414+2
-8	.624+4	.575+4	.512+4	.426+4	.350+4	.209+4	.139+4	.517+3	.149+3	.405+2
-7	.274+4	.270+4	.253+4	.223+4	.192+4	.129+4	.919+3	.415+3	.135+3	.384+2
	TORR=.5									
-12	.144+5	.126+5	.106+5	.821+4	.645+4	.337+4	.214+4	.639+3	.164+3	.420+2
-11	.135+5	.121+5	.102+5	.795+4	.625+4	.329+4	.209+4	.633+3	.163+3	.419+2
-10	.120+5	.111+5	.944+4	.743+4	.588+4	.314+4	.200+4	.620+3	.161+3	.418+2
-9	.905+4	.884+4	.773+4	.621+4	.498+4	.276+4	.178+4	.586+3	.157+3	.414+2
-8	.532+4	.553+4	.504+4	.422+4	.348+4	.208+4	.139+4	.517+3	.149+3	.405+2
-7	.240+4	.261+4	.249+4	.221+4	.191+4	.128+4	.917+3	.415+3	.135+3	.384+2
	TORR=1.									
-12	.117+5	.119+5	.103+5	.809+4	.638+4	.334+4	.212+4	.638+3	.164+3	.420+2
-11	.111+5	.115+5	.995+4	.783+4	.619+4	.327+4	.208+4	.632+3	.163+3	.419+2
-10	.999+4	.106+5	.925+4	.733+4	.582+4	.312+4	.199+4	.619+3	.161+3	.418+2
-9	.774+4	.849+4	.759+4	.614+4	.494+4	.275+4	.178+4	.585+3	.157+3	.414+2
-8	.468+4	.534+4	.496+4	.418+4	.345+4	.207+4	.139+4	.516+3	.149+3	.405+2
-7	.215+4	.254+4	.246+4	.219+4	.190+4	.128+4	.916+3	.415+3	.135+3	.384+2
	TORR=5.									
-12	.591+4	.100+5	.946+4	.763+4	.610+4	.325+4	.208+4	.633+3	.163+3	.419+2
-11	.565+4	.965+4	.913+4	.739+4	.592+4	.317+4	.203+4	.626+3	.163+3	.419+2
-10	.521+4	.892+4	.851+4	.694+4	.558+4	.303+4	.195+4	.614+3	.161+3	.418+2
-9	.425+4	.724+4	.702+4	.583+4	.474+4	.268+4	.174+4	.581+3	.157+3	.414+2
-8	.276+4	.461+4	.462+4	.399+4	.334+4	.203+4	.137+4	.513+3	.149+3	.405+2
-7	.134+4	.221+4	.230+4	.211+4	.185+4	.126+4	.906+3	.413+3	.135+3	.384+2
	TORR=10.									
-12	.404+4	.903+4	.892+4	.731+4	.589+4	.317+4	.203+4	.627+3	.163+3	.419+2
-11	.385+4	.869+4	.861+4	.708+4	.572+4	.310+4	.199+4	.621+3	.162+3	.419+2
-10	.355+4	.804+4	.802+4	.665+4	.539+4	.296+4	.191+4	.609+3	.160+3	.418+2
-9	.291+4	.651+4	.662+4	.560+4	.459+4	.262+4	.171+4	.576+3	.156+3	.414+2
-8	.193+4	.414+4	.436+4	.384+4	.324+4	.199+4	.135+4	.511+3	.148+3	.405+2
-7	.963+3	.199+4	.218+4	.203+4	.180+4	.124+4	.896+3	.412+3	.135+3	.384+2

TABLE IV: NORMALIZED THERMAL RESPONSE FROM X-RAYS IN STAINLESS STEEL WITH NEON GAS PROTECTION

log Δt (sec)	BLACKBODY TEMPERATURE (KEV) .1	.2	.3	.4	.5	.75	1.	2.	5.	10.
	TORR=.1									
-12	.946+4	.103+5	.892+4	.707+4	.567+4	.300+4	.194+4	.598+3	.162+3	.417+2
-11	.899+4	.991+4	.860+4	.684+4	.550+4	.294+4	.190+4	.592+3	.161+3	.417+2
-10	.813+4	.913+4	.799+4	.641+4	.517+4	.280+4	.182+4	.582+3	.159+3	.415+2
-9	.636+4	.735+4	.657+4	.538+4	.439+4	.248+4	.163+4	.554+3	.155+3	.412+2
-8	.390+4	.464+4	.431+4	.368+4	.309+4	.189+4	.128+4	.494+3	.147+3	.403+2
-7	.181+4	.222+4	.216+4	.195+4	.172+4	.118+4	.861+3	.403+3	.134+3	.383+2
	TORR=.5									
-12	.309+4	.584+4	.524+4	.436+4	.372+4	.207+4	.142+4	.493+3	.154+3	.409+2
-11	.297+4	.560+4	.505+4	.422+4	.361+4	.203+4	.139+4	.490+3	.154+3	.409+2
-10	.275+4	.516+4	.470+4	.396+4	.339+4	.194+4	.134+4	.484+3	.152+3	.408+2
-9	.227+4	.415+4	.386+4	.334+4	.290+4	.174+4	.121+4	.469+3	.149+3	.405+2
-8	.150+4	.264+4	.256+4	.232+4	.208+4	.137+4	.988+3	.433+3	.143+3	.397+2
-7	.753+3	.128+4	.131+4	.128+4	.120+4	.903+3	.697+3	.367+3	.131+3	.378+2
	TORR=1.									
-12	.168+4	.387+4	.340+4	.289+4	.256+4	.149+4	.107+4	.427+3	.148+3	.402+2
-11	.160+4	.370+4	.327+4	.279+4	.248+4	.146+4	.105+4	.426+3	.147+3	.401+2
-10	.147+4	.339+4	.303+4	.261+4	.233+4	.140+4	.102+4	.422+3	.146+3	.400+2
-9	.120+4	.269+4	.246+4	.219+4	.199+4	.126+4	.932+3	.413+3	.144+3	.398+2
-8	.787+3	.167+4	.162+4	.153+4	.144+4	.102+4	.777+3	.389+3	.138+3	.391+2
-7	.399+3	.800+3	.834+3	.859+3	.856+3	.699+3	.572+3	.339+3	.129+3	.374+2
	TORR=5.									
-12	.299+3	.796+3	.630+3	.550+3	.541+3	.401+3	.365+3	.285+3	.128+3	.378+2
-11	.270+3	.755+3	.600+3	.528+3	.523+3	.394+3	.361+3	.285+3	.128+3	.378+2
-10	.231+3	.678+3	.544+3	.486+3	.488+3	.381+3	.352+3	.284+3	.128+3	.377+2
-9	.167+3	.511+3	.420+3	.394+3	.411+3	.349+3	.333+3	.281+3	.127+3	.376+2
-8	.933+2	.286+3	.251+3	.264+3	.298+3	.298+3	.299+3	.273+3	.124+3	.371+2
-7	.406+2	.121+3	.120+3	.152+3	.193+3	.234+3	.251+3	.252+3	.118+3	.358+2
	TORR=10.									
-12	.104+3	.175+3	.134+3	.130+3	.149+3	.158+3	.185+3	.235+3	.120+3	.365+2
-11	.853+2	.166+3	.127+3	.125+3	.144+3	.156+3	.184+3	.235+3	.120+3	.365+2
-10	.645+2	.149+3	.115+3	.115+3	.136+3	.152+3	.182+3	.234+3	.119+3	.364+2
-9	.408+2	.111+3	.880+2	.943+2	.117+3	.144+3	.176+3	.233+3	.119+3	.363+2
-8	.204+2	.610+2	.514+2	.648+2	.901+2	.130+3	.166+3	.227+3	.117+3	.359+2
-7	.810+1	.249+2	.241+2	.399+2	.640+2	.110+3	.149+3	.213+3	.111+3	.347+2

TABLE V: NORMALIZED THERMAL RESPONSE FROM X-RAYS IN STAINLESS STEEL WITH XENON GAS PROTECTION

logΔt (sec)	BLACKBODY TEMPERATURE (KEV) .1	.2	.3	.4	.5	.75	1.	2.	5.	10.
	TORR=.1									
-12	.576+4	.306+4	.242+4	.209+4	.181+4	.125+4	.898+3	.418+3	.138+3	.391+2
-11	.541+4	.294+4	.235+4	.204+4	.178+4	.123+4	.889+3	.416+3	.137+3	.391+2
-10	.482+4	.273+4	.222+4	.195+4	.171+4	.120+4	.871+3	.412+3	.137+3	.390+2
-9	.367+4	.224+4	.191+4	.172+4	.154+4	.111+4	.822+3	.401+3	.135+3	.387+2
-8	.220+4	.149+4	.136+4	.129+4	.121+4	.931+3	.714+3	.375+3	.132+3	.381+2
-7	.101+4	.752+3	.745+3	.770+3	.772+3	.658+3	.540+3	.325+3	.123+3	.365+2
	TORR=.5									
-12	.148+3	.836+2	.939+2	.143+3	.190+3	.239+3	.243+3	.222+3	.106+3	.332+2
-11	.142+3	.814+2	.926+2	.142+3	.189+3	.238+3	.243+3	.222+3	.106+3	.332+2
-10	.131+3	.773+2	.900+2	.139+3	.187+3	.236+3	.241+3	.221+3	.106+3	.331+2
-9	.107+3	.672+2	.831+2	.132+3	.180+3	.230+3	.237+3	.219+3	.105+3	.330+2
-8	.703+2	.487+2	.682+2	.116+3	.163+3	.215+3	.224+3	.212+3	.103+3	.326+2
-7	.346+2	.267+2	.454+2	.867+2	.129+3	.181+3	.195+3	.196+3	.985+2	.316+2
	TORR=1.									
-12	.230+1	.174+1	.796+1	.259+2	.484+2	.860+2	.107+3	.143+3	.849+2	.287+2
-11	.223+1	.171+1	.790+1	.258+2	.483+2	.858+2	.106+3	.142+3	.849+2	.287+2
-10	.210+1	.164+1	.780+1	.255+2	.480+2	.854+2	.106+3	.142+3	.847+2	.287+2
-9	.179+1	.147+1	.751+1	.249+2	.471+2	.842+2	.105+3	.141+3	.843+2	.286+2
-8	.124+1	.112+1	.673+1	.232+2	.445+2	.807+2	.101+3	.138+3	.832+2	.283+2
-7	.649+0	.655+0	.515+1	.192+2	.381+2	.716+2	.916+2	.129+3	.798+2	.276+2
	TORR=5.									
-12	.314-12	.187-9	.498-3	.597-1	.446+0	.143+1	.306+1	.199+2	.312+2	.151+2
-11	.310-12	.185-9	.497-3	.596-1	.446+0	.143+1	.305+1	.199+2	.312+2	.151+2
-10	.304-12	.182-9	.494-3	.594-1	.445+0	.142+1	.305+1	.199+2	.311+2	.151+2
-9	.284-12	.174-9	.485-3	.588-1	.441+0	.141+1	.302+1	.198+2	.311+2	.151+2
-8	.234-12	.151-9	.459-3	.571-1	.432+0	.139+1	.296+1	.195+2	.309+2	.150+2
-7	.149-12	.106-9	.391-3	.522-1	.405+0	.130+1	.278+1	.187+2	.302+2	.148+2
	TORR=10.									
-12	.313-27	.383-20	.263-7	.309-3	.119-1	.414-1	.132+0	.513+1	.162+2	.987+1
-11	.310-27	.380-20	.262-7	.308-3	.119-1	.414-1	.132+0	.513+1	.162+2	.986+1
-10	.304-27	.374-20	.261-7	.308-3	.119-1	.413-1	.131+0	.512+1	.162+2	.986+1
-9	.286-27	.357-20	.256-7	.305-3	.118-1	.411-1	.131+0	.511+1	.162+2	.985+1
-8	.241-27	.312-20	.244-7	.297-3	.116-1	.403-1	.128+0	.506+1	.161+2	.983+1
-7	.158-27	.219-20	.210-7	.275-3	.110-1	.383-1	.121+0	.493+1	.159+2	.974+1

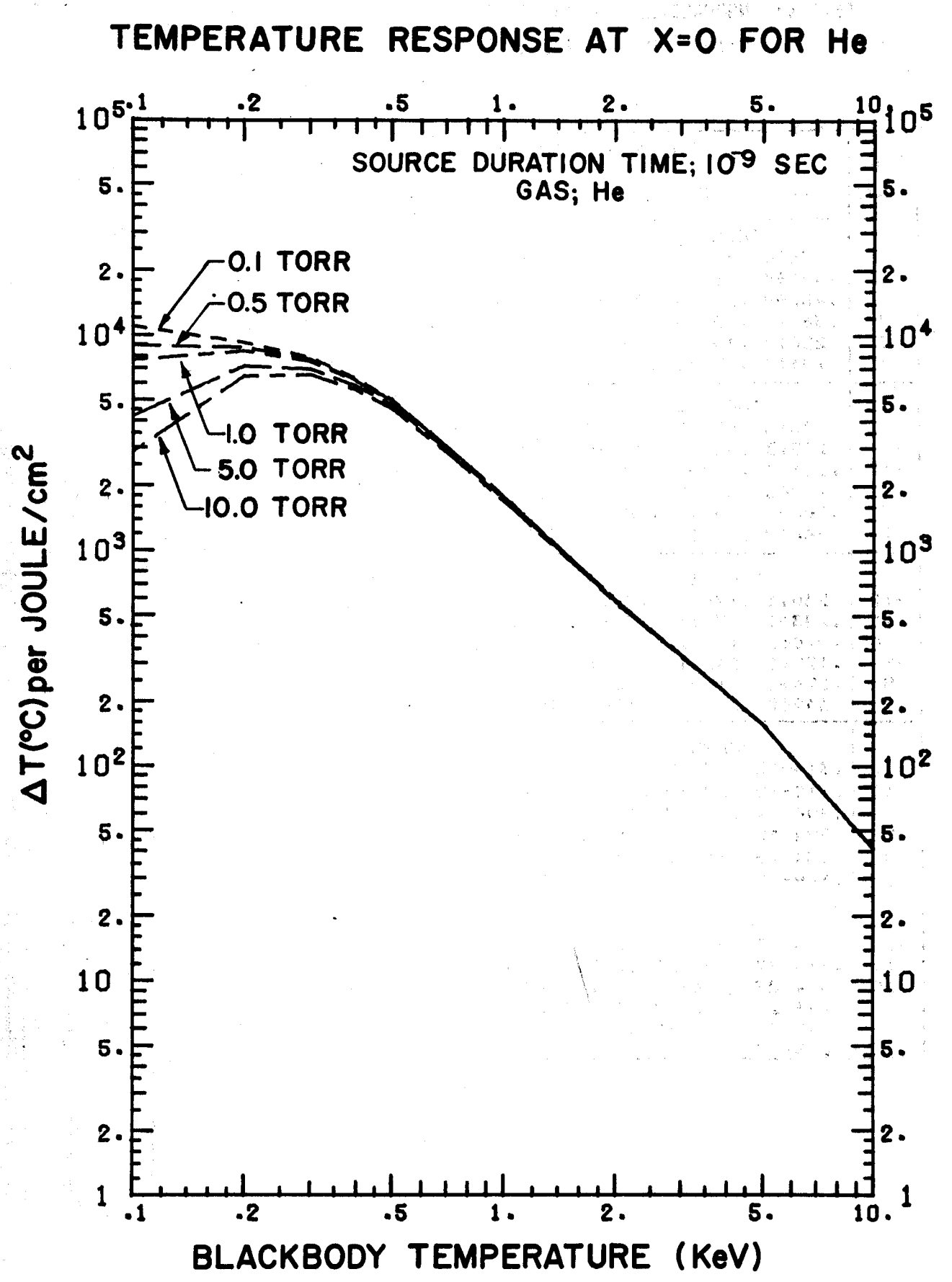
TEMPERATURE RESPONSE AT X=0 FOR He
SOURCE DURATION TIME; 10⁻⁹ SEC
GAS; He
0.1 TORR
0.5 TORR
1.0 TORR
5.0 TORR
10.0 TORR
ΔT(°C) per JOULE/cm²
BLACKBODY TEMPERATURE (KeV)
.1
.2
.5
1.
2.
5.
10.
10⁵
5.
2.
10⁴
5.
2.
10³
5.
2.
10²
5.
2.
10
5.
2.
1

FIGURE 27

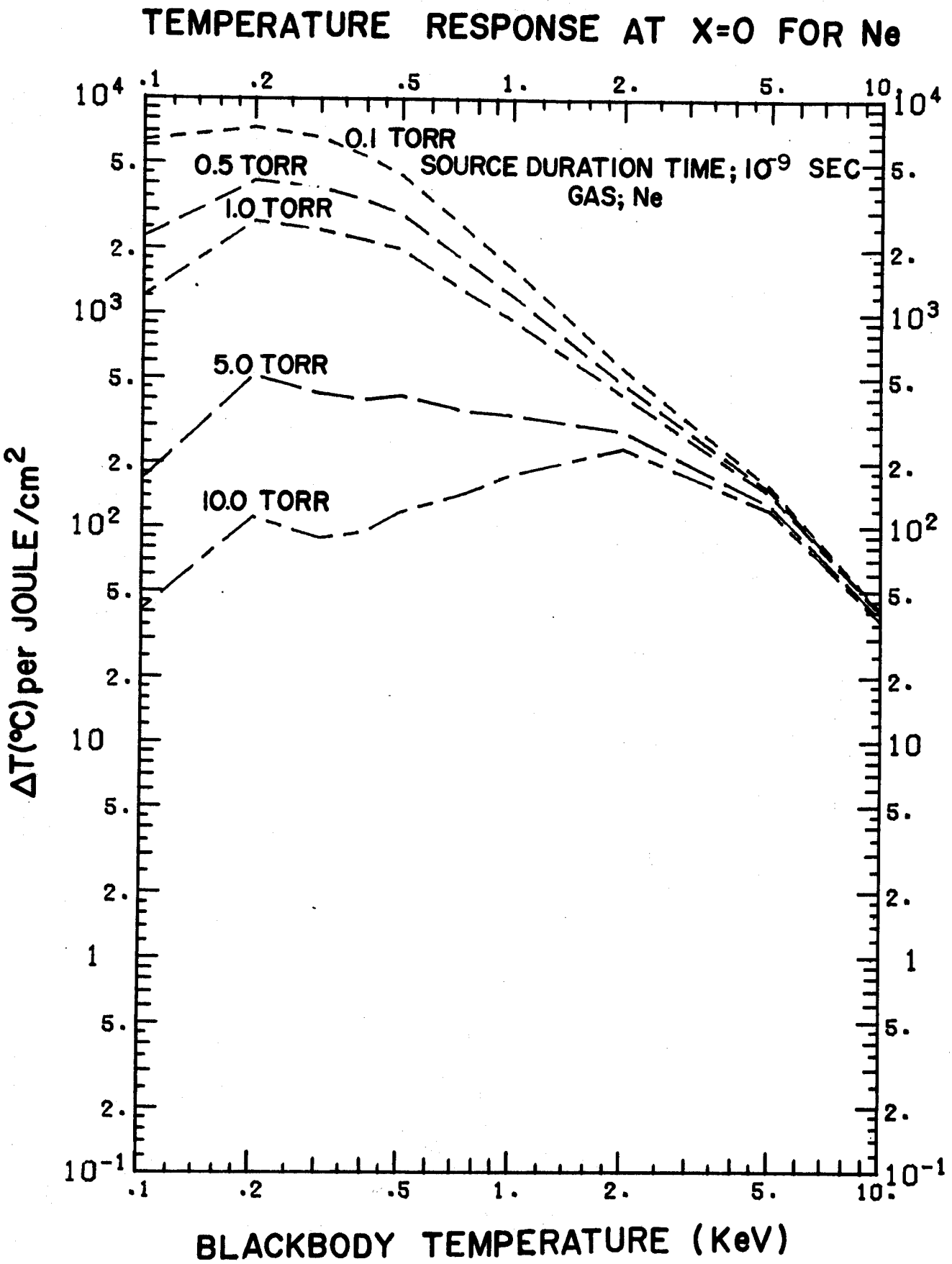
TEMPERATURE RESPONSE AT X=0 FOR Ne
0.1 TORR
0.5 TORR
1.0 TORR
5.0 TORR
10.0 TORR
SOURCE DURATION TIME; 10⁻⁹ SEC
GAS; Ne
ΔT(°C) per JOULE/cm²
BLACKBODY TEMPERATURE (KeV)
.1
.2
.5
1.
2.
5.
10.
10⁴
10³
10²
10
1
10⁻¹

FIGURE 28

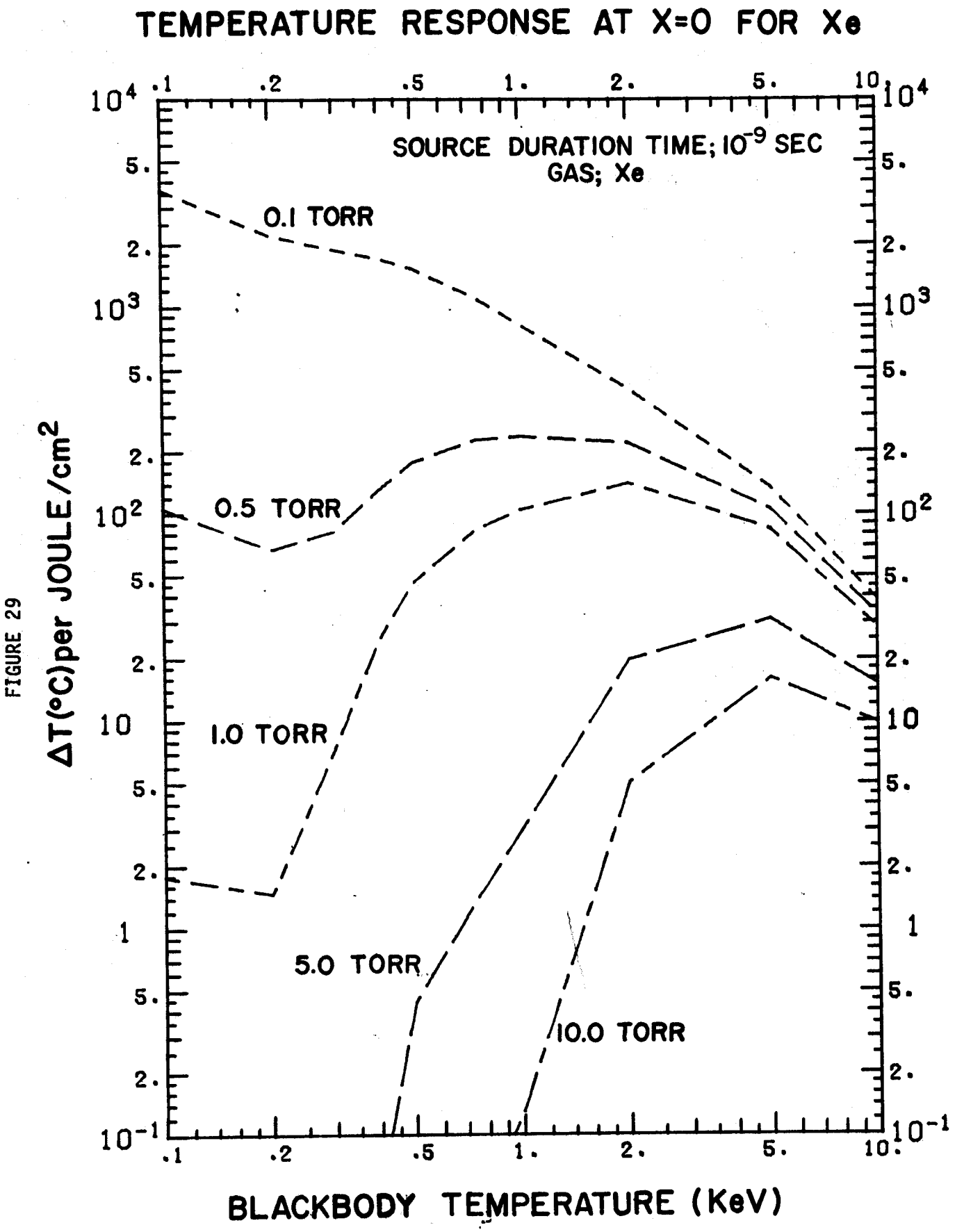
TEMPERATURE RESPONSE AT X=0 FOR Xe
SOURCE DURATION TIME; 10^{-9} SEC
GAS; Xe
0.1 TORR
0.5 TORR
1.0 TORR
5.0 TORR
10.0 TORR
$\Delta T(°C)$ per JOULE/cm^2
BLACKBODY TEMPERATURE (KeV)
.1
.2
.5
1.
2.
5.
10
10^4
10^3
10^2
10
1
10^{-1}

FIGURE 29

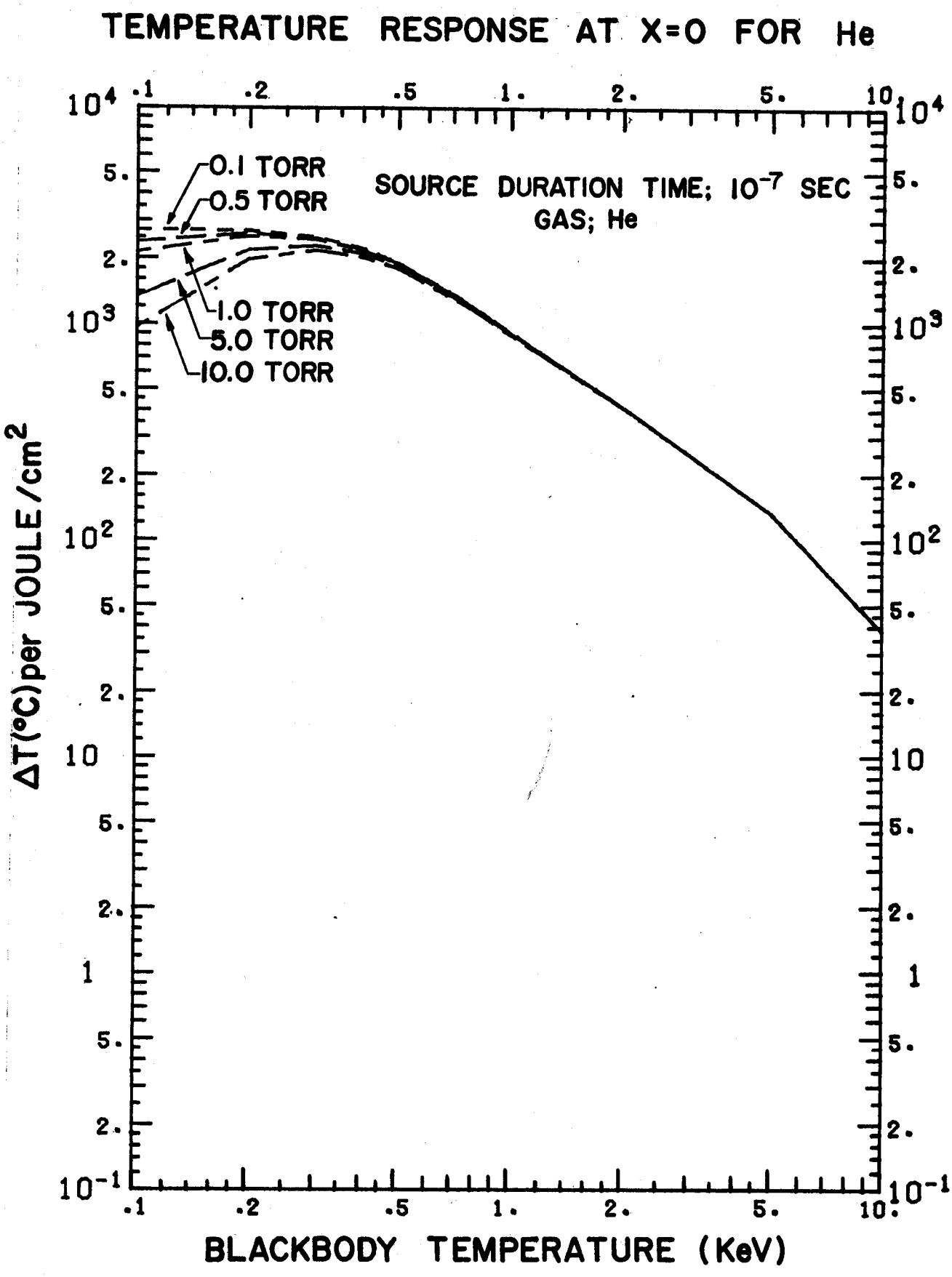
TEMPERATURE RESPONSE AT X=0 FOR He
SOURCE DURATION TIME; 10^{-7} SEC
GAS; He
0.1 TORR
0.5 TORR
1.0 TORR
5.0 TORR
10.0 TORR
$\Delta T(°C)$ per JOULE/cm^2
BLACKBODY TEMPERATURE (KeV)
.1
.2
.5
1.
2.
5.
10.
10^4
10^3
10^2
10
1
10^{-1}

FIGURE 30

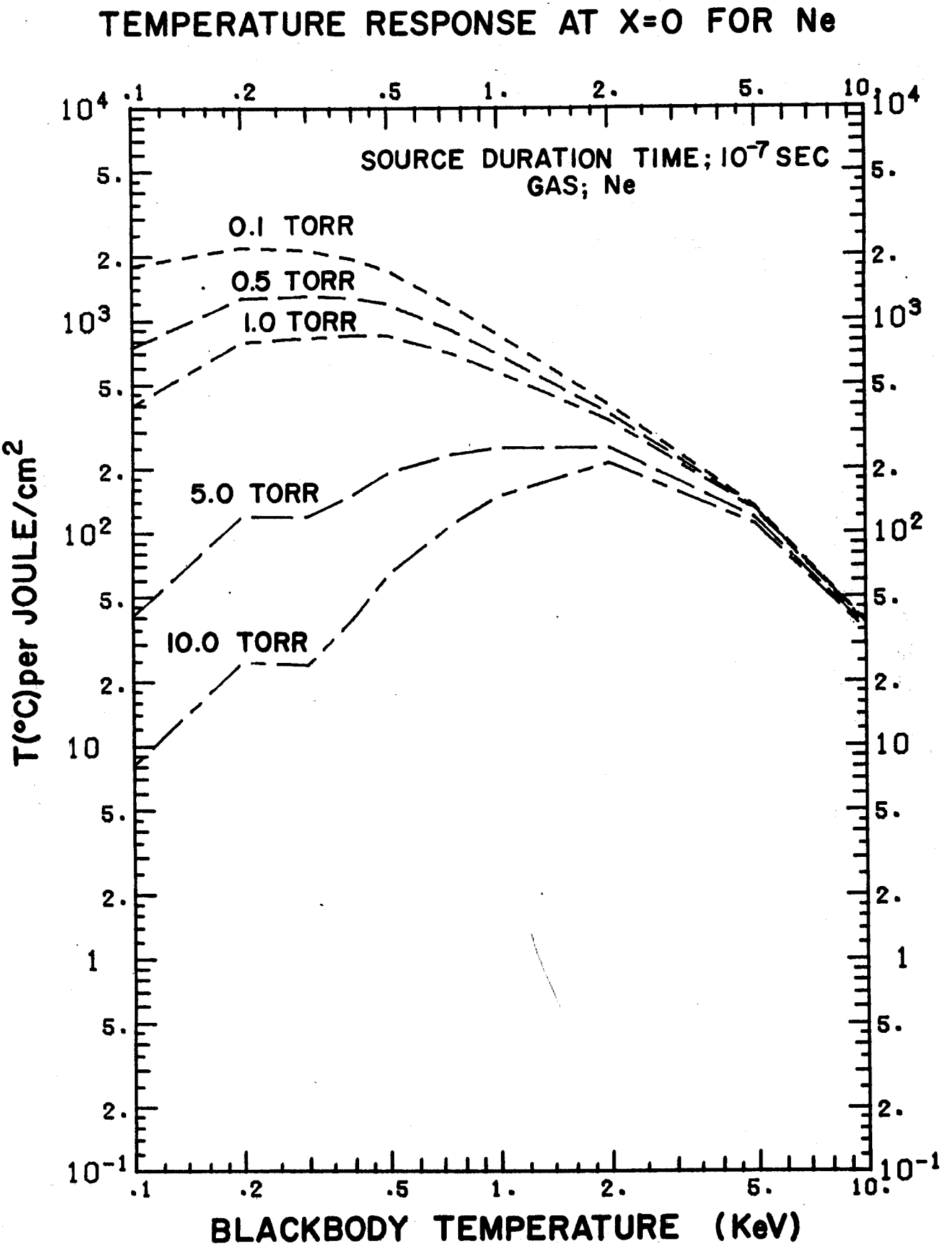
TEMPERATURE RESPONSE AT X=0 FOR Ne
SOURCE DURATION TIME; 10^{-7} SEC
GAS; Ne
0.1 TORR
0.5 TORR
1.0 TORR
5.0 TORR
10.0 TORR
T(°C)per JOULE/cm^2
BLACKBODY TEMPERATURE (KeV)
.1
.2
.5
1.
2.
5.
10
10^4
10^3
10^2
10
1
10^{-1}

FIGURE 31

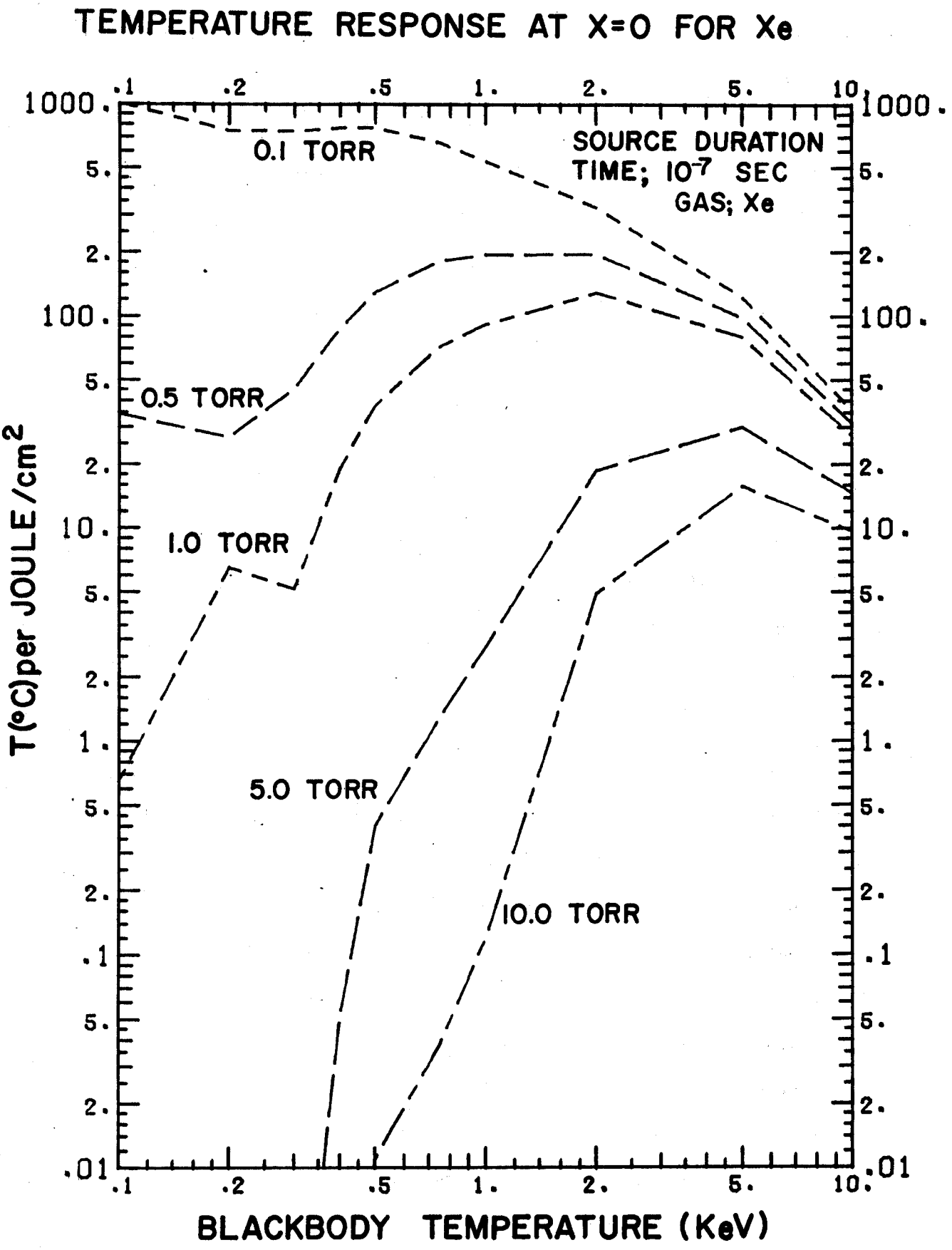
TEMPERATURE RESPONSE AT X=0 FOR Xe
SOURCE DURATION TIME; 10^{-7} SEC
GAS; Xe
0.1 TORR
0.5 TORR
1.0 TORR
5.0 TORR
10.0 TORR
T(°C)per JOULE/cm^2
BLACKBODY TEMPERATURE (KeV)
1000.
100.
10.
1.
.1
.01
.1
.2
.5
1.
2.
5.
10.

FIGURE 32

It can be seen from Figures 27 through 32 that increasing the source duration time from 10^{-9} seconds to 10^{-7} seconds reduces the temperature rise by a factor of about 3. The irregularities in the xenon and neon curves at higher gas densities are due to combinations of absorption edges in the gas and stainless steel (see Figure 2). It is clear from these curves that using a layer of high Z gas to protect the first wall results in a substantial decrease in the temperature response from soft X-rays.

Figures 33 and 34 show the significant variation in temperature response with the atomic number of gas used for protection. Greater pressures for the lighter gases will be required to achieve the same result as will xenon. Neon at a pressure of 1.0 torr reduces the temperature pulse by a factor 2 to 5 for blackbody spectra up to 5 keV. Helium provides only a small reduction in the thermal response (about 30%) for blackbody spectra at 0.1 keV and almost no reduction for blackbody spectra greater than 0.5 keV. On the other hand, xenon almost eliminates the X-ray temperature response for soft spectra, and provides some reduction in response for the harder X-rays. It is clear that high atomic number gases (xenon) offer more protection against temperature increases due to X-rays, particularly for softer spectra.

The influence of source duration time is best shown in Figure 35. for a gas pressure of 0.1 torr and Figure 36 for gas pressure of 1.0 torr. It is obvious that for hard X-ray spectra there is almost no reduction from adiabatic response as the source duration time increases. For soft X-ray spectra, the reduction is very small due to the poor thermal conductivity of stainless steel. For materials with higher thermal conductivity (like copper), significant temperature reductions have been predicted as the source duration increases.[3]

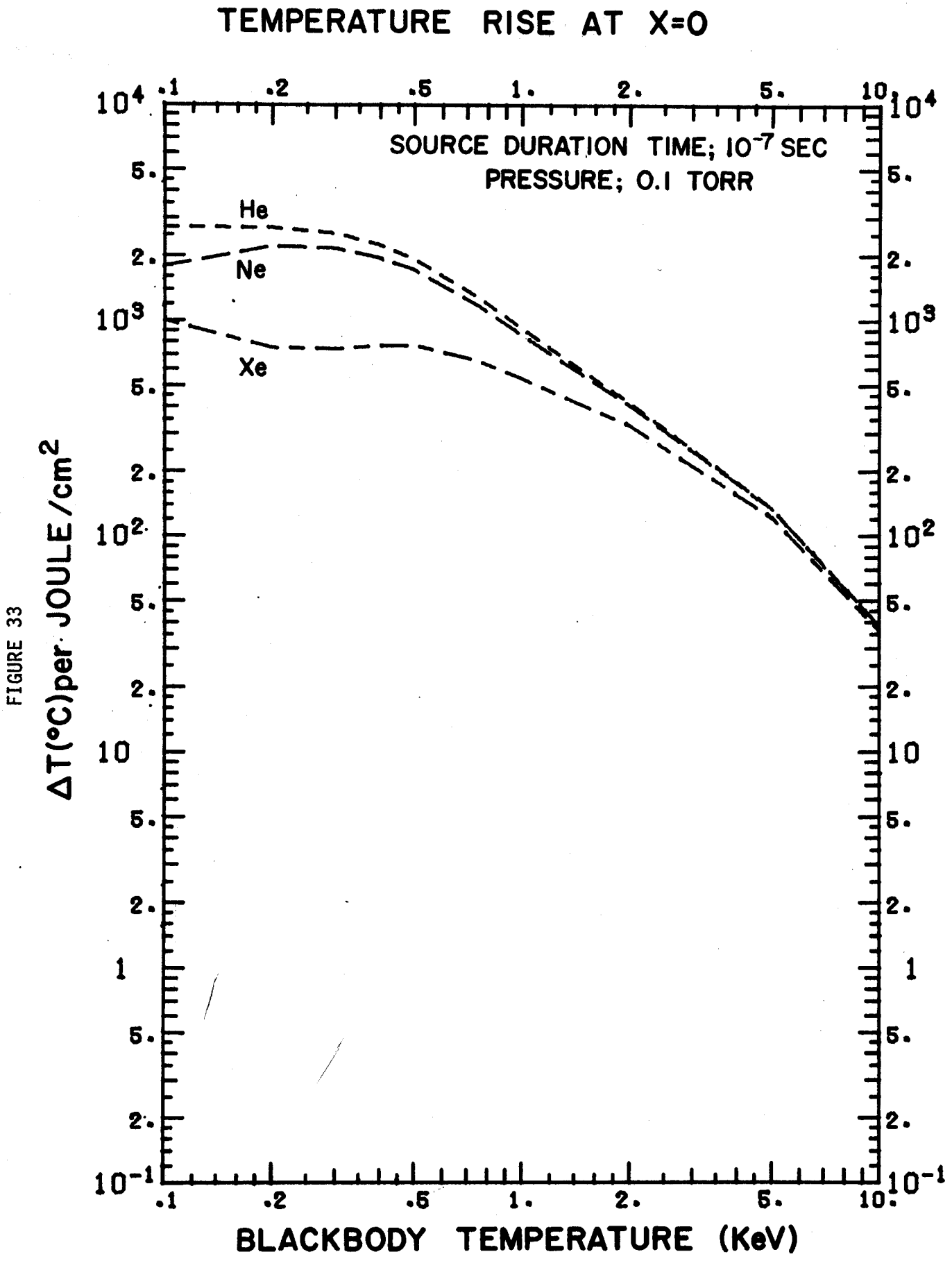
TEMPERATURE RISE AT X=0
SOURCE DURATION TIME; 10^{-7} SEC
PRESSURE; 0.1 TORR
He
Ne
Xe
$\Delta T(°C)$ per JOULE/cm^2
BLACKBODY TEMPERATURE (KeV)
.1
.2
.5
1.
2.
5.
10.
10^4
10^3
10^2
10
1
10^{-1}

FIGURE 33

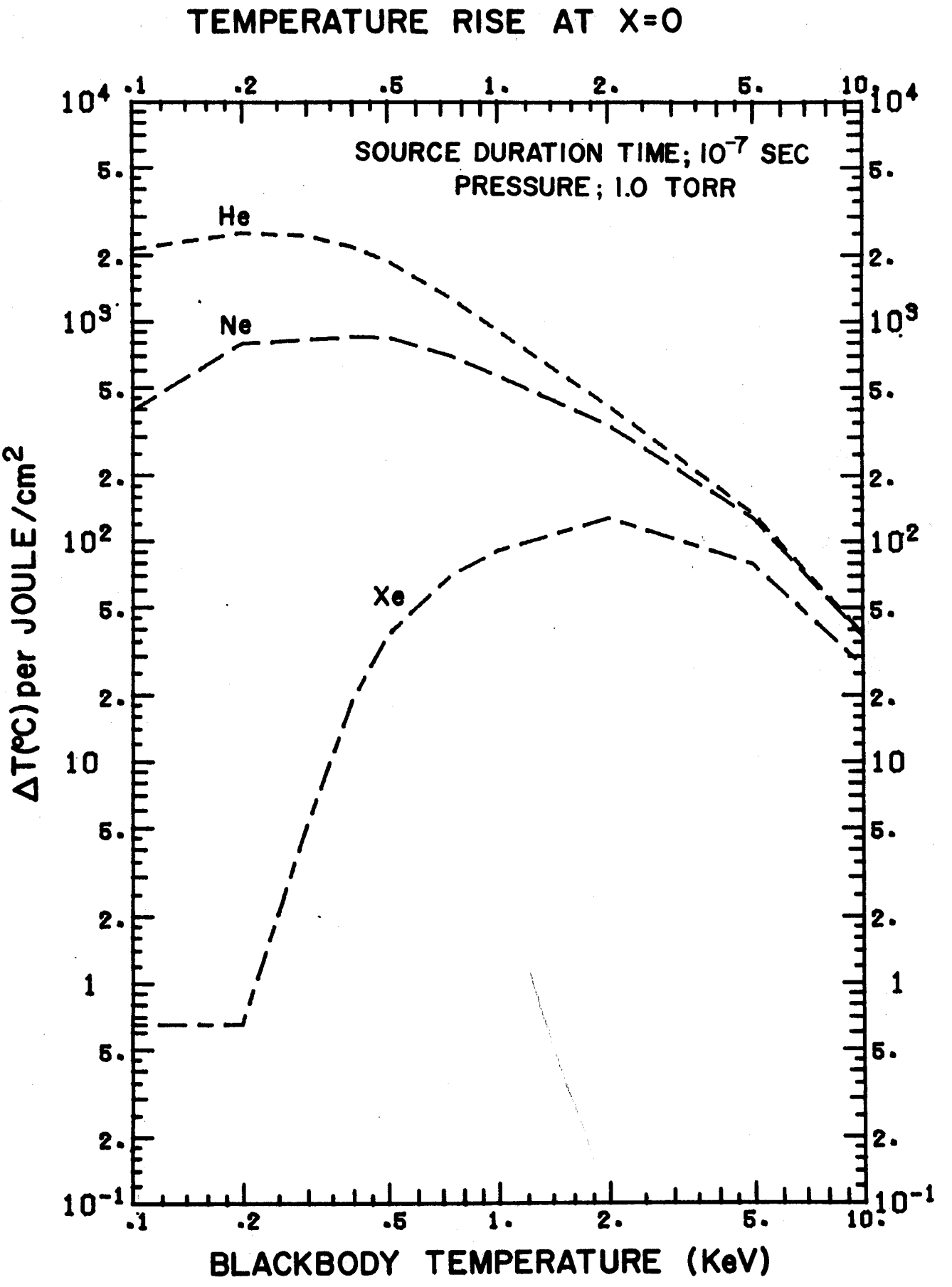
TEMPERATURE RISE AT X=0
SOURCE DURATION TIME; 10^{-7} SEC
PRESSURE; 1.0 TORR
He
Ne
Xe
ΔT(°C) per JOULE/cm²
BLACKBODY TEMPERATURE (KeV)
.1
.2
.5
1.
2.
5.
10
10^4
10^3
10^2
10
1
10^{-1}

FIGURE 34

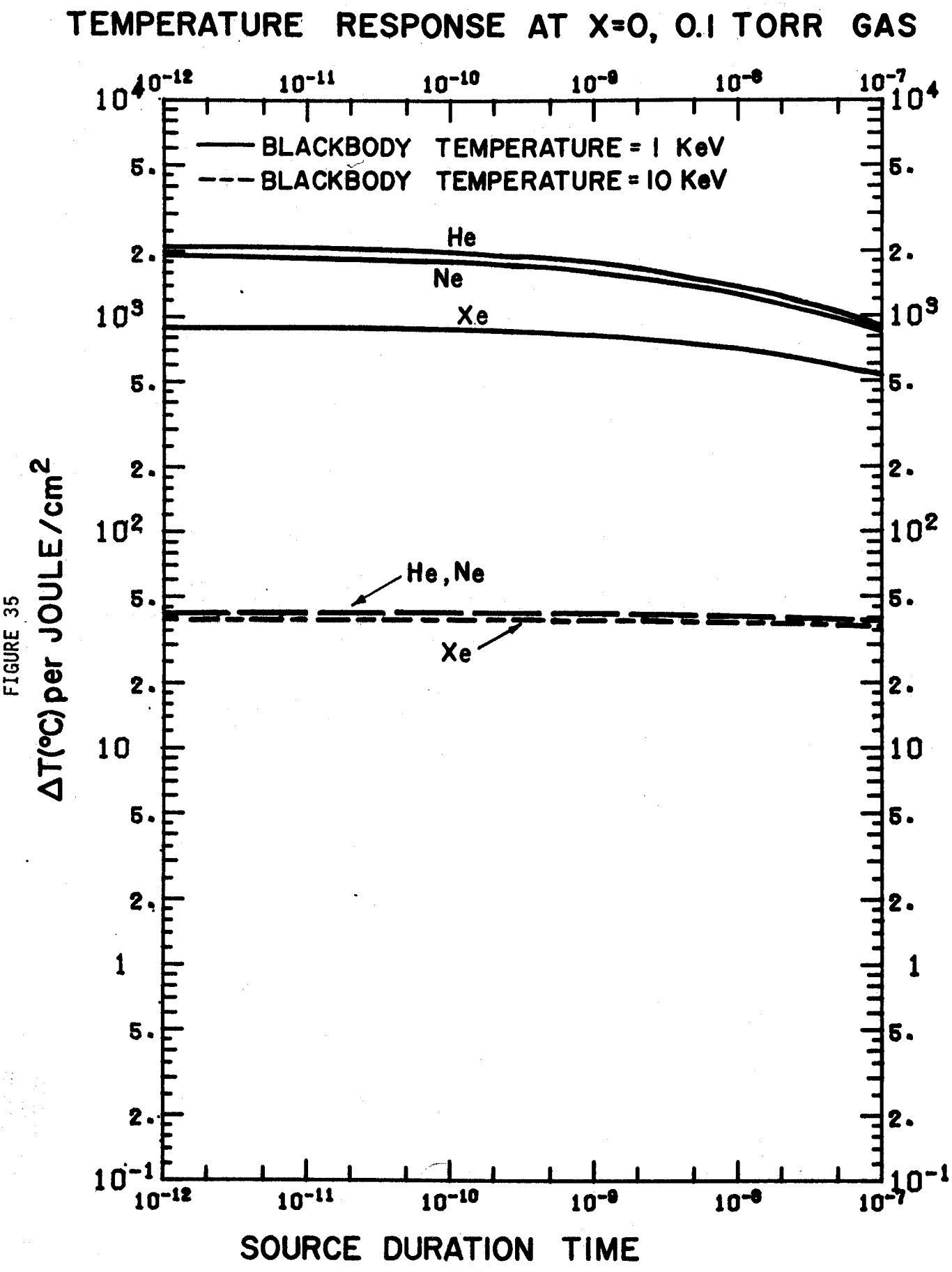
TEMPERATURE RESPONSE AT X=0, 0.1 TORR GAS
BLACKBODY TEMPERATURE = 1 KeV
BLACKBODY TEMPERATURE = 10 KeV
He
Ne
Xe
He, Ne
Xe
ΔT(°C) per JOULE/cm²
SOURCE DURATION TIME
10⁻¹² 10⁻¹¹ 10⁻¹⁰ 10⁻⁹ 10⁻⁸ 10⁻⁷
10⁴ 5. 2. 10³ 5. 2. 10² 5. 2. 10 5. 2. 1 5. 2. 10⁻¹

FIGURE 35

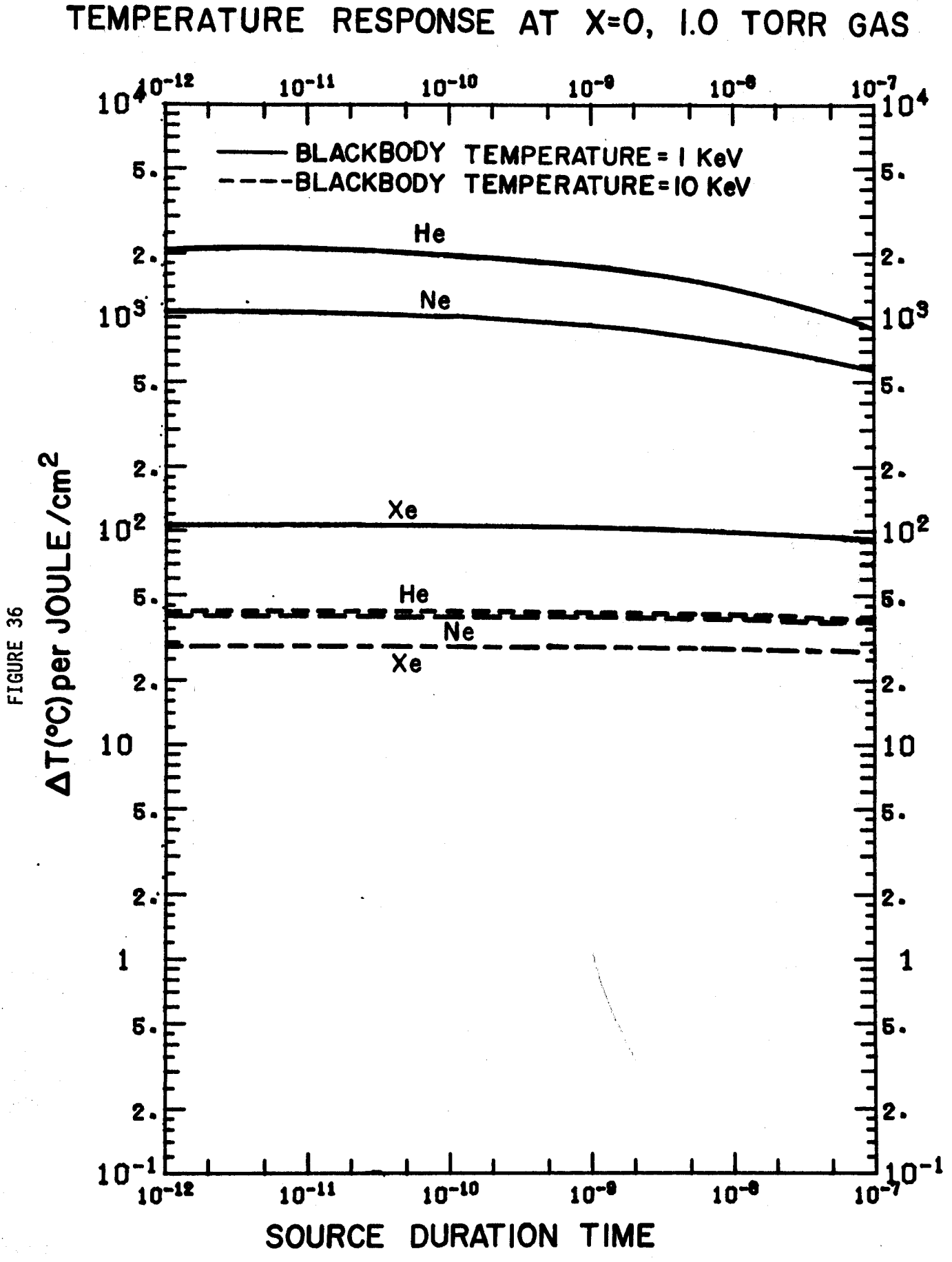
TEMPERATURE RESPONSE AT X=0, 1.0 TORR GAS
BLACKBODY TEMPERATURE = 1 KeV
BLACKBODY TEMPERATURE = 10 KeV
He
Ne
Xe
He
Ne
Xe
ΔT(°C) per JOULE/cm²
SOURCE DURATION TIME
10⁻¹²
10⁻¹¹
10⁻¹⁰
10⁻⁹
10⁻⁸
10⁻⁷
10⁴
10³
10²
10
1
10⁻¹

FIGURE 36

To summarize the results of the X-ray parameter study, three-dimensional plots are presented for the stainless steel temperature response at four pressures (0.1, 1.0, 5.0, 10.0 torr) in Figures 37 through 39. Each plot shows the temperature response as a function of the source duration and blackbody temperature. It is clearly seen in these figures that increasing the gas pressure of helium from 0.1 torr to 10 torr has little influence on the temperature response. A more interesting case is that for neon at 10.0 torr, where the effect of the absorption edges can be seen (see Figure 2). By comparing the case of 10.0 torr neon with that of 0.5 torr xenon, one observes the two plots give almost the same temperature rise.

8. Conclusions

These calculations have shown that the large temperature excursions in metals from the rapid deposition of X-rays and ions are approximately twice as large in stainless steel as in copper. In both materials, 0.5 torr of neon reduces the temperature pulse by a factor of 1/2 when compared to the case of no gas, reiterating the role of a buffer gas as a first wall protection scheme.

When comparing the three inert gases, He, Ne and Xe, one finds that helium is relatively transparent to most of the thermonuclear X-ray radiation at gas pressures compatible with laser fusion (i.e., less than 10 torr). On the other hand, the use of Xe at pressures greater than a few torr can effectively stop all the X-rays below 1 keV.

FIGURE 37

TEMPERATURE RESPONSE FOR HELIUM BUFFER GAS AT X=0

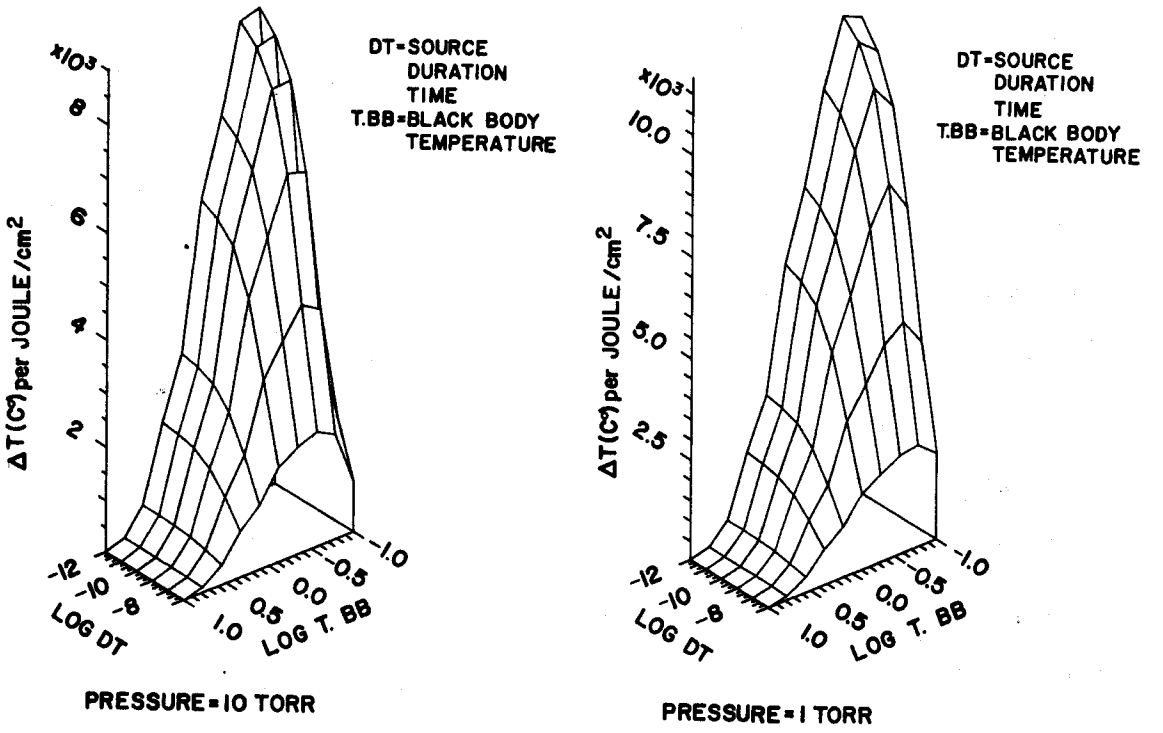

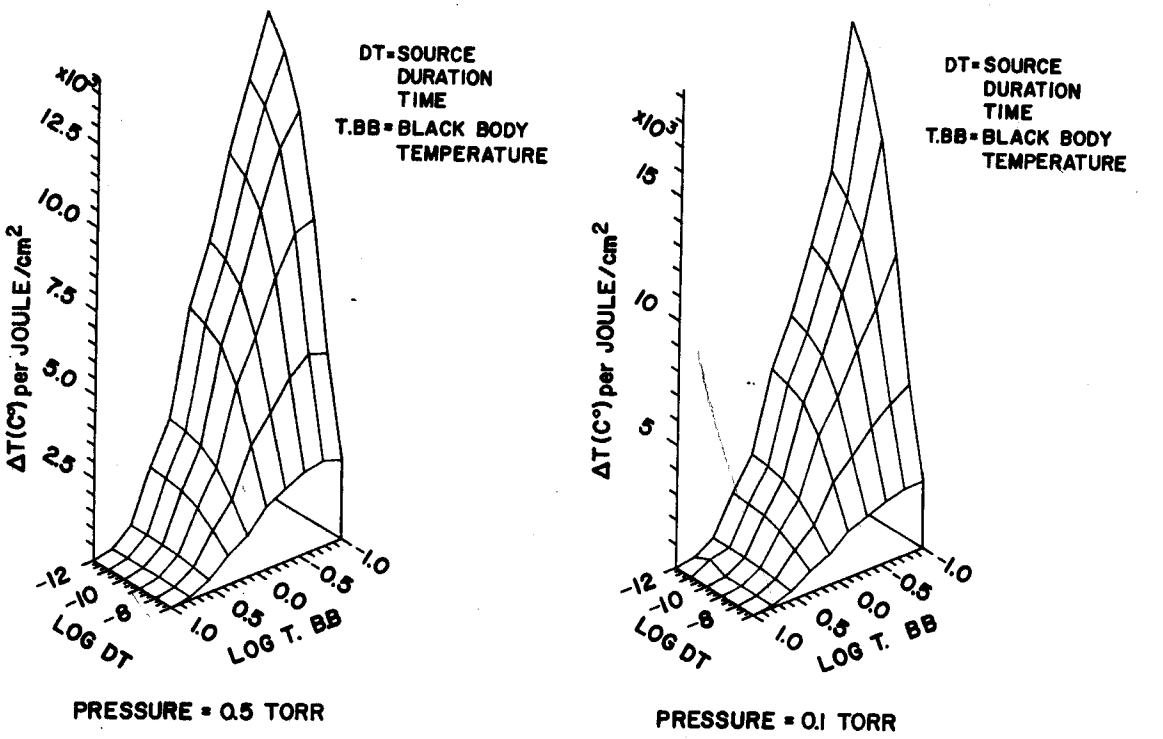

FIGURE 38

TEMPERATURE RESPONSE FOR NEON BUFFER GAS AT X=0

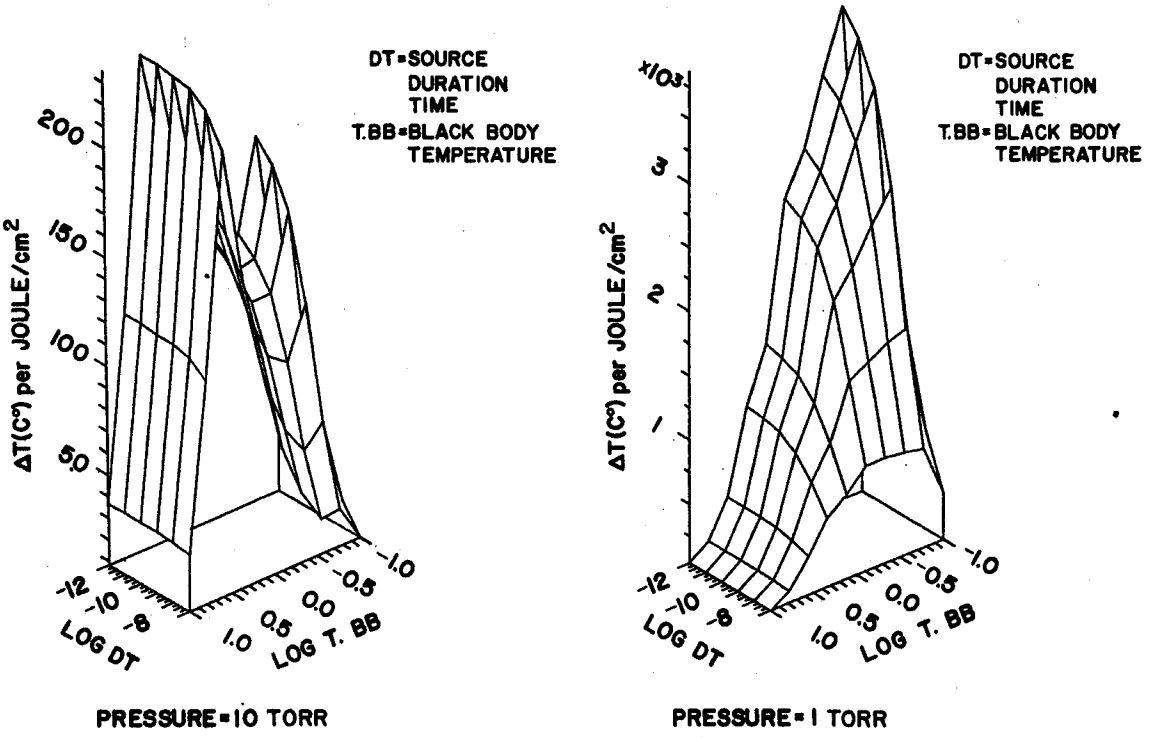

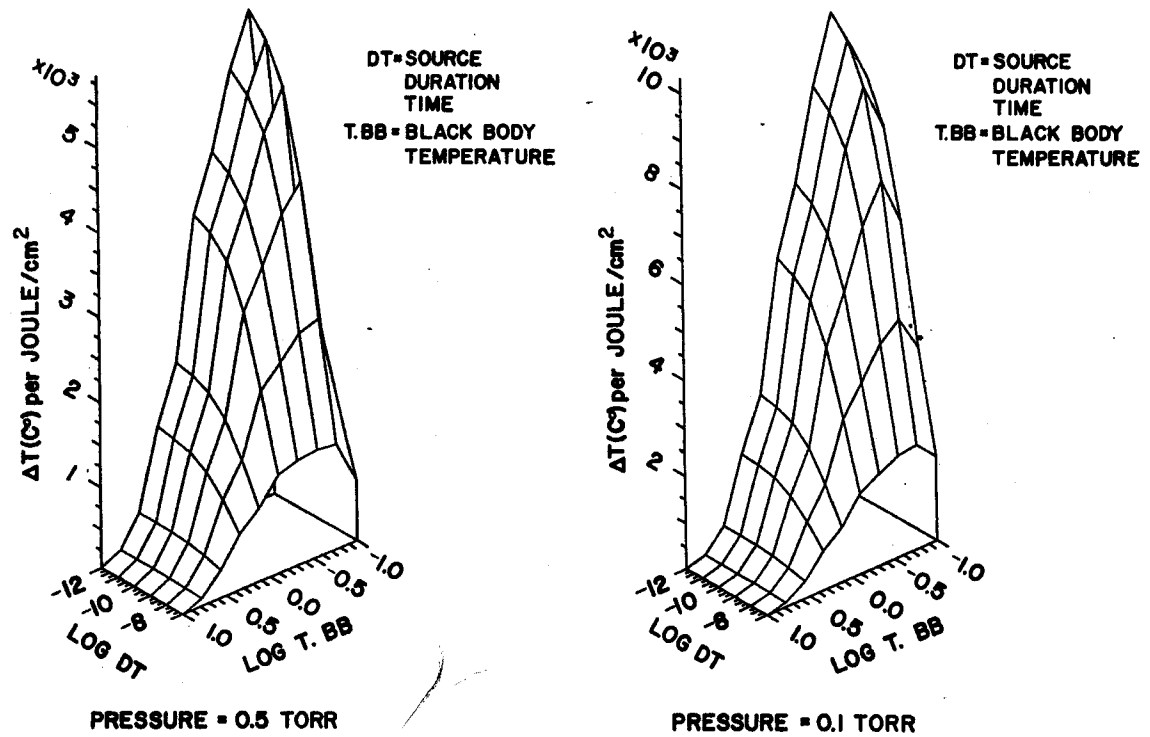

FIGURE 39

TEMPERATURE RESPONSE FOR XENON BUFFER GAS AT X=0

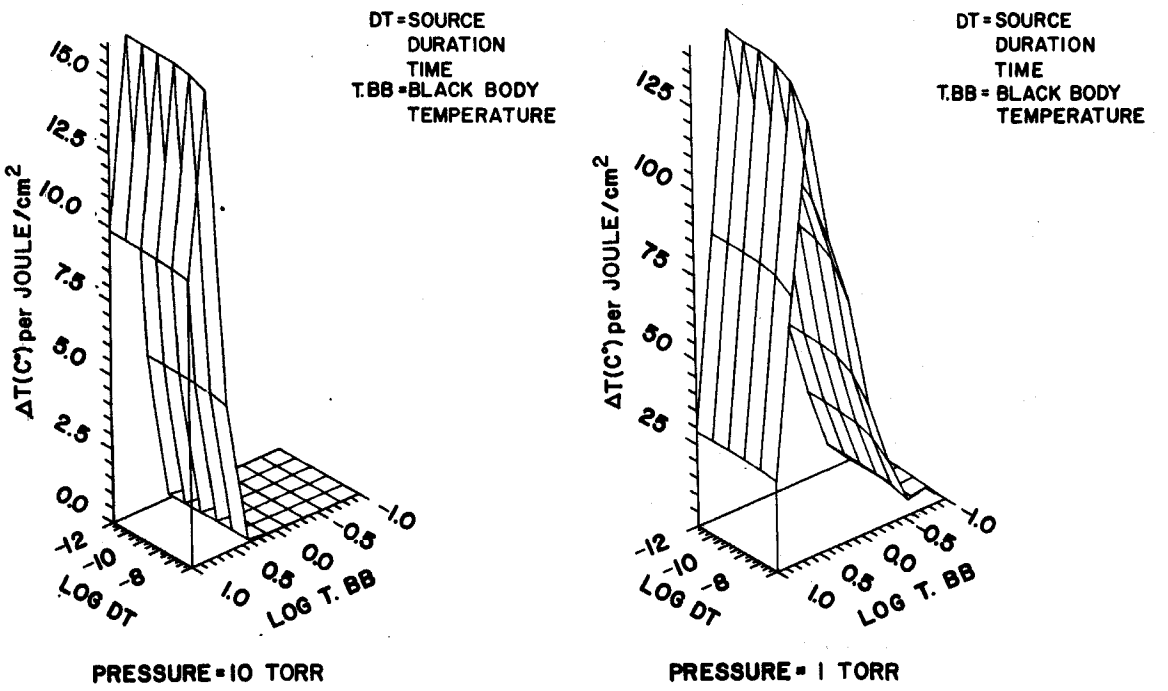

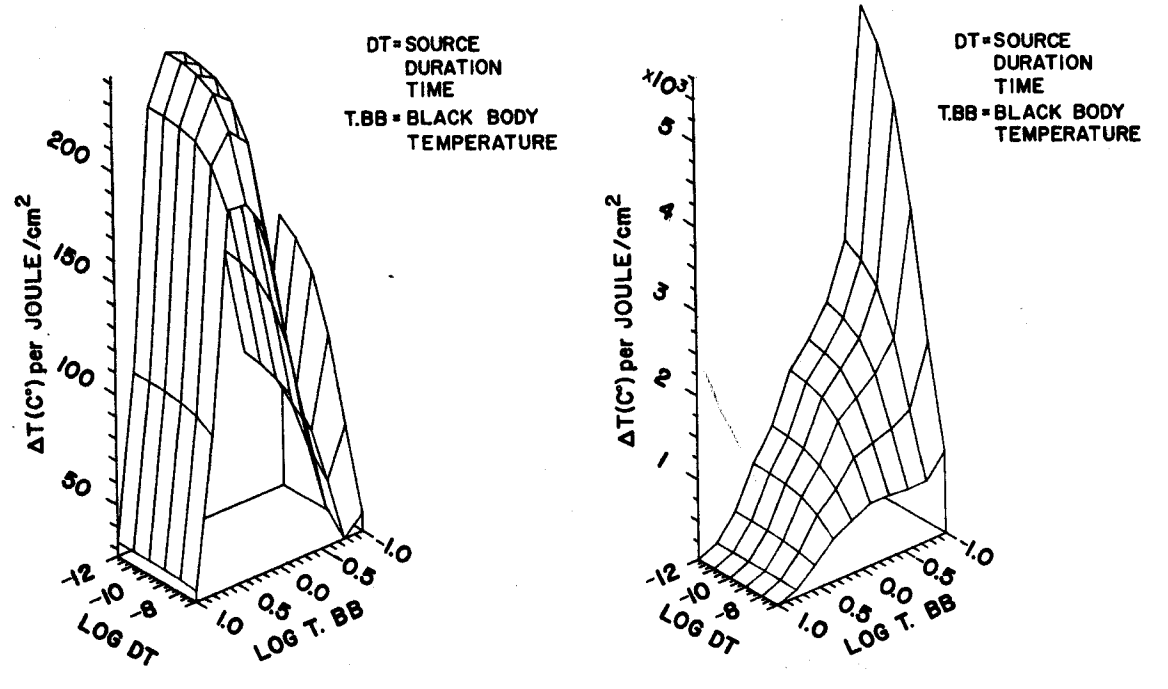

It was found that X-ray pulse duration of less than 10^{-7} seconds was not important in determining the final temperature increase in steel. This conclusion is slightly modified if higher thermal diffusivity metals like Cu are used.

The use of as little as 0.5 torr of Ne in a seven meter radius chamber can reduce the displacement damage per pulse by a factor of 2. Not only is the magnitude of the damage reduced, but the spacial profile is significantly modified. The peak damage region now occurs closer to the surface.

The gas protection scheme described here shows stainless steel reactor chambers of about 7 meters could be used if at least 10-torr meters of high atomic number gas is used. Hydrodynamic calculations including gas reradiations could be coupled to these results to give a more accurate temperature history.

Acknowledgment

Support for this work was provided by the U.S. Department of Energy.

References

1. T. O. Hunter, G. L. Kulcinski, "Description of the Response of Materials to Pulsed Thermonuclear Radiation (Part 1)," UWFDM-196, Nuc. Eng. Dept., University of Wisconsin-Madison, March 1977.

2. T. O. Hunter, G. L. Kulcinski, "Description of the Response of Materials to Pulsed Thermonuclear Radiation (Part II)," UWFDM-217, Nuc. Eng. Dept., University of Wisconsin-Madison, October 1977.

3. T. O. Hunter, and G. L. Kulcinski, "Description of the Response of Materials to Pulsed Thermonuclear Radiation (Part III)," UWFDM-232, Nuc. Eng. Dept., University of Wisconsin-Madison, April 1978.

4. T. O. Hunter, and G. L. Kulcinski, "T-DAMEN, a Computer Code for Analysis of Transient Radiation Damage," UWFDM-247, Nuc. Eng. Dept. University of Wisconsin-Madison, May 1978.

5. David K. Brice, "Three-Parameter Formula for the Electronic Stopping Cross Section at Non-relativistic Velocities," Vol. 6, No. 5, Physical Review A, November 1972.

6. David K. Brice, "Ion Implantation Range and Energy Depositions, Vol. 1, IFI/Plenum, New York.

7. R. Behrish, "First Wall Erosion in Fusion Reactors," Nuclear Fusion, No. 12, 1972, P. 695.

8. J. Lindhard, et al., "Range Concepts and Heavy Ion Ranges," Mat. Fys. Medd. Dan. Vid. Selsk, 33, No. 14 (1963).

9. D. G. Doran, et al., "Report of the Working Group on Displacement Models and Procedures for Damage Calculations," HEDL-TME 73-76, Hanford Engineering Development Laboratory, December 1973.